

Holographic Wilson loops in Lifshitz-like backgrounds

Dmitry S. Ageev,^a Irina Ya. Aref'eva,^a Anastasia A. Golubtsova^b and Eric Gourgoulhon^c

^a*Steklov Mathematical Institute, Russian Academy of Sciences,
Gubkina str. 8, 119991, Moscow, Russia*

^b*Bogoliubov Laboratory of Theoretical Physics, JINR,
141980 Dubna, Moscow region, Russia*

^c*Laboratoire Univers et Théories, Observatoire de Paris, CNRS, Université Paris Diderot
5 place Jules Janssen, 92190 Meudon, France*

E-mail: arefeva@mi.ras.ru, golubtsova@theor.jinr.ru,
eric.gourgoulhon@obspm.fr

ABSTRACT: In this paper, we continue to investigate nonequilibrium properties of the anisotropic quark-gluon plasma produced in heavy ion collisions within the holographic approach. We evaluate spatial Wilson loops using both static and time-dependent dual backgrounds. The anisotropic time-dependent plasma is dual to the Lifshitz-Vaidya background, while we use a black brane in the Lifshitz-like spacetime for a finite temperature plasma in equilibrium. To probe the system we calculate Wilson loops oriented in different spatial directions. We find that anisotropic effects in the Lifshitz-like backgrounds are more visible for the Wilson loops lying in the transversal plane unlike the Wilson loops with partially longitudinal orientation. We also observe that these Wilson loops are more sensitive to the parameter controlling the anisotropy of the metric. We compute the string tension and the pseudopotential at different temperatures for the static quark-gluon plasma. We also compare the thermalization times of spatial Wilson loops with the thermalization times of entanglement entropy and two-point correlation functions. We note that the thermalization of 2-point correlators is faster compared to Wilson loops, the thermalization of which is faster than the thermalization of entanglement entropy. Increasing the anisotropy we decrease the thermalization times of all these observables keeping the order of their thermalization.

KEYWORDS: quark-gluon plasma, holography, black holes and branes, Lifshitz-like metric, thermalization, anisotropy

Contents

1	Introduction	2
2	Set Up	3
2.1	Wilson loops	3
2.2	The Lifshitz-like metrics	5
3	Spatial Wilson loops in a time-independent background	6
3.1	Wilson loops on the xy_1 -plane	7
3.1.1	Rectangular strip infinite along the y_1 -direction	7
3.1.2	Rectangular strip infinite along the x -direction	9
3.2	Wilson loop on the y_1y_2 -plane	11
3.3	Spatial string tension dependence on the orientation	13
4	Spatial Wilson loops in a time-dependent background	16
4.1	Wilson loops on the xy_1 -plane	16
4.1.1	Rectangular strip infinite along the y_1 -direction	16
4.1.2	Rectangular strip infinite along the x -direction	18
4.2	Wilson loop on the y_1y_2 -plane	22
5	Thermalization times	24
5.1	Thermalization times of spacial Wilson loops	24
5.2	Thermalization times of different observables	25
6	Conclusions	27
A	Some details on numerical solutions	29
A.1	Case 1	29
A.2	Case 2	29
A.3	Case 3	29
B	Asymptotics for static pseudopotentials	31
B.1	Rectangular strip in xy_1 -plane infinite along the y_1 -direction	31
B.2	Rectangular strip in the xy_1 -plane infinite along the x -direction	33
B.3	Rectangular strip in y_1y_2 -plane infinite along the y_2 -direction	34
C	Thermalization times of holographic two-point correlators and entanglement entropy	35
C.1	Thermalization time of two-point correlators	35
C.2	Thermalization time of entanglement entropy	35

1 Introduction

Wilson loops are known to play a key role as fundamental probes of gauge theories, in particular QCD. Owing to Wilson loops one can define many important quantities, for instance, we can derive the potential of a quark-antiquark interaction from the expectation value of the space-time rectangular Wilson loop. At the same time, expectation values of Wilson loops are used to characterize properties of QGP produced in heavy ion collisions. In particular, with the help of Wilson loops one can perform the analysis of radiative parton energy loss, quarkonium suppression, etc.[1].

In the lattice QCD the Wilson loops are the prime observables and their expectation values are defined non-perturbatively [2]. One can also determine expectation values of Wilson loops in the framework of perturbative QCD after suitable renormalization [3]. In this paper we study spatial Wilson loops as well as its thermalization in the holographic approach. To study Wilson loops in anisotropic media produced in heavy-ion collisions we use the dual background with anisotropic scaling. Expectation values of Wilson loops within the gauge/gravity duality have been calculated for the strongly coupled $\mathcal{N} = 4$ super Yang-Mills theory [4–7]. The string dual description of the real QCD is unknown in spite of a lot of performed effort to find it [8–10]. However, suitable "bottom-up" holographic QCD models matching with experimental and lattice results have been proposed in [11–19].

It is widely appreciated that the gauge/gravity duality provides a powerful tool for studying dynamics of the strong coupling system, in particular, the quark-gluon plasma (QGP) produced in heavy-ion collisions (HIC) [1]. The QGP is created after a very short time after the collision, about $0.2 \div 1 fm/c$, and the holographic duality is rather suitable to describe this period of evolution [20, 21]. The holographic approach is convenient to incorporate anisotropic properties of QGP created in heavy-ion collisions [22, 23].

Main idea of this approach is to use natural prescriptions of the general AdS/CFT correspondence trying to recover non-perturbative QCD phenomena, in particular non-perturbative vacuum phenomena, finite temperature, high-dense and non-zero chemical potential phenomena. In this strategy, fitting parameters are ones specifying the form of the 5-dimensional metric. The 5-dimensional metric is supposed to be a solution of Einstein equations with a suitable matter content, not necessary related with string theory. According to the holographic approach, thermalization of physical 4-dimensional models corresponds to the process of the formation of the black hole/brane in the 5-dimensional bulk induced by an injection of some matter from the boundary. In particular, the scenario of a heavy-ion collision can be represented here as a shock wave collision in which a trapped surface is formed [24]–[33]. After the collision the shocks slowly decay, leaving the plasma described by hydrodynamics. The creation of the black hole can be also described by an infalling shell [34] propagating in the 5-dimensional bulk. A gravitational collapse of a thin shell to a black hole can provide a gravitational dual description of the thermalization process [35]–[37]. A successive holographic model is supposed to describe several real phenomena.

It has been shown that holographic estimations of the total multiplicity can fit the experimental data at high energies using the so-called Lifshitz-like metric for certain values

of critical exponents [38]. String duals of Lifshitz-like fixed points were suggested in [39, 40] and the thermodynamics and the hydrodynamic behavior of their dual field theories were studied in [40]. Lifshitz-like metrics also occur as the IR limit for the anisotropic background suggested for studies of QGP in [41]. We note that the Lifshitz-like backgrounds differ from the Lifshitz metric [42] by the anisotropic scaling of spatial coordinates. In [38] the HIC has been holographically modeled by shock wall collisions in the Lifshitz-like background. Vaidya solutions in the Lifshitz-like spacetimes have been found in [44]. The thermalization time of the 2-point correlators and the thermalization of holographic entanglement entropy have been estimated in [43, 44].

As already mentioned, the information about processes during HIC can be read off from the expectation values of Wilson loops. Thus, it is also natural to study the behaviour of Wilson loops during the HIC within the same holographic model we used to fit the energy dependence of total multiplicity. In particular, it is reasonable to investigate thermalization of Wilson loops and their behaviour in the end of the thermalization process.

In the present work we calculate spatial Wilson loops in the Lifshitz-like background which represent rectangles with two infinitely long sides and two sides of finite lengths. By virtue of the Lifshitz-like metric possessing a spatial anisotropy, the expectation values of Wilson loops depend on the orientation of the corresponding loop. Further, we study potentials and its evolution during the thermalization process. It should be noted that Wilson loops in static Lifshitz spacetimes have been considered in [47]–[52]. Various physical quantities, in particular expectation values of Wilson loops, have been calculated holographically using string actions in static anisotropic backgrounds, see for example [23], [53]–[65], and refs therein.

The paper is organized as the following. In Sec. 2 we briefly discuss the holographic description of Wilson loops, gravitational backgrounds and the notations. In Sec. 3 we analyze the static Wilson loops as well as calculate pseudopotentials and string tensions for different orientations of Wilson loop. In Sec. 4 we study the nonequilibrium dynamics of the same oriented Wilson loops and present the results. In Sec. 5 the thermalization time of Wilson loops is estimated and we compare it with the thermalization times of the entanglement entropy and two-point correlation functions. We conclude with a discussion of our results and further directions.

2 Set Up

2.1 Wilson loops

In this work we consider rectangular Wilson loops. As already noticed, Wilson loops contain the information about the force between quarks. Following the holographic approach [4, 5] the expectation value of the Wilson loop in the fundamental representation calculated on the gravity side reads as:

$$W[C] = \langle \text{Tr}_F e^{i \oint_C dx_\mu A_\mu} \rangle = e^{-S_{string}[C]}, \quad (2.1)$$

where C is a contour on the boundary, F means the fundamental representation (we will omit this symbol in what follows), S is the minimal action of the string hanging from the

contour C in the bulk. The Nambu-Goto action can be represented as

$$S_{string} = \frac{1}{2\pi\alpha'} \int d\sigma^1 d\sigma^2 \sqrt{-\det(h_{\alpha\beta})}, \quad (2.2)$$

with the induced metric of the world-sheet $h_{\alpha\beta}$ given by

$$h_{\alpha\beta} = g_{MN} \partial_\alpha X^M \partial_\beta X^N, \quad (2.3)$$

where $\alpha, \beta = 1, 2$. In (2.3) g_{MN} is the background metric, $M, N = 1, \dots, 5$, $X^M = X^M(\sigma^1, \sigma^2)$ specify the string worldsheet and σ^1, σ^2 parametrize the worldsheet.

The potential of the interquark interaction can be extracted from the rectangular time-like Wilson loop of size $T \times X$, i.e. the loop in which one side is infinite along the time direction, and the other is along the spatial one,

$$W(T, X) = \langle \text{Tr} e^{i \oint_{T \times X} dx_\mu A_\mu} \rangle \sim e^{-V(X)T}. \quad (2.4)$$

A similar operator to probe QCD is the spatial rectangular Wilson loop of size $X \times Y$. The following relation for spatial Wilson loops¹ for large Y

$$W(X, Y) = \langle \text{Tr} e^{i \oint_{X \times Y} dx_\mu A_\mu} \rangle = e^{-\mathcal{V}(X)Y}, \quad (2.5)$$

defines the so called pseudopotential \mathcal{V} . We note, that for large Y the behavior of $W(X, Y)$ is different from the behaviour of the time-like one.

The pseudopotential can be straightforwardly extracted from the string action (2.2) as follows

$$\mathcal{V}(X) = \frac{S_{string}}{Y}. \quad (2.6)$$

As it is known from the QCD lattice calculations the spatial Wilson loops obey the area law at all temperature, i.e.

$$\mathcal{V}(X) \sim \sigma_s X, \quad (2.7)$$

where σ_s defines the spatial string tension

$$\sigma_s = \lim_{X \rightarrow \infty} \frac{\mathcal{V}(X)}{X}. \quad (2.8)$$

The quantity σ_s differs from the usual string tension which is defined from time-like Wilson-loops. By virtue to the non-Abelian Stokes formula equal time spatial Wilson loops [66] are related with the spatial components of the energy-momentum tensor and by this reason σ_s is also called the magnetic string tension. Spatial Wilson loops have been studied on the lattice [67, 68], analytically [69], and also within the gauge/gravity duality [70, 71].

¹Note that we take $X < Y$ for real calculations, where X is large, but not infinite.

2.2 The Lifshitz-like metrics

We start from the gravitational theory given by the action [44]

$$S = \int d^5x \sqrt{|g|} \left(R[g] + \Lambda - \frac{1}{2}(\partial\phi)^2 - \frac{1}{4}e^{\lambda\phi}F_{(2)}^2 \right), \quad (2.9)$$

where ϕ is the dilaton field, $F_{(2)}$ is $U(1)$ gauge field, λ is a dilaton coupling constant, and Λ is the negative cosmological constant. The corresponding Einstein equations of motion are

$$R_{mn} = -\frac{\Lambda}{3}g_{mn} + \frac{1}{2}(\partial_m\phi)(\partial_n\phi) + \frac{1}{2}e^{\lambda\phi}F_{mp}F_n^p - \frac{1}{12}e^{\lambda\phi}F_{(2)}^2g_{mn}. \quad (2.10)$$

The scalar field equation and Maxwell's equation read

$$\square\phi = \frac{1}{4}\lambda e^{\lambda\phi}F_{(2)}^2, \text{ with } \square\phi = \frac{1}{\sqrt{|g|}}\partial_m(g^{mn}\sqrt{|g|}\partial_n\phi), \quad (2.11)$$

$$D_m(e^{\lambda\phi}F^{mn}) = 0. \quad (2.12)$$

We will study the thermalization of Wilson loops in gravity backgrounds that are asymptotic to the 5d Lifshitz-like geometries [39, 40]

$$ds^2 = 2\pi\alpha' \left(\frac{-dt^2 + dx^2}{z^2} + \frac{dy_1^2 + dy_2^2}{z^{2/\nu}} + \frac{dz^2}{z^2} \right), \quad (2.13)$$

where ν is the critical exponent. Note, that in (2.13) to keep the standard dimension for the metric we put the factor $2\pi\alpha'$ in front of the metric and we assume that all lengths in different directions are dimensionless² $[\ell_z] = [\ell_x] = [\ell_{y_1}] = [\ell_{y_2}] = (\alpha')^0$.

The dilaton and gauge fields are given by

$$\phi = \phi(r), \quad e^{\lambda\phi} = \mu e^{4r}, \quad (2.15)$$

$$F_{(2)} = \frac{1}{2}q dy_1 \wedge dy_2, \quad (2.16)$$

where q and μ are constants. One can see that the background (2.13) with $\nu = 1$ comes to be the 5-dimensional AdS spacetime. As already mentioned, the choice of this metric is motivated by the fact that holographic estimations of the total multiplicity performed in this background reproduce the experimental dependence of the multiplicity on the energy [38].

²Note that here instead of $2\pi\alpha'$ one can put the square dimension parameter R^2 , and taking the metric in the form

$$ds^2 = \frac{R^2}{z^2}(-dt^2 + dx^2 + dz^2) + \frac{R^{2/\nu}}{z^{2/\nu}}(dy_1^2 + dy_2^2), \quad (2.14)$$

one can deal with dimensional coordinates.

The non-zero temperature generalization of (2.13) as a solution to (2.9) was constructed without changing the field ansatz in [44]³:

$$ds^2 = 2\pi\alpha' \left(\frac{-f(z)dt^2 + dx^2}{z^2} + \frac{dy_1^2 + dy_2^2}{z^{2/\nu}} + \frac{dz^2}{z^2 f(z)} \right), \quad (2.17)$$

with the blackening function

$$f = 1 - mz^{2+2/\nu}. \quad (2.18)$$

For $\nu = 1$ the background (2.17) with (2.18) represents the metric of the AdS black brane.

To study the thermalization process, corresponding to the black brane formation in the dual language, we will also use the Lifshitz-Vaidya solution⁴ [44]:

$$ds^2 = 2\pi\alpha' \left(-\frac{f(v, z)dv^2 - 2dv dz + dx^2}{z^2} + \frac{dy_1^2 + dy_2^2}{z^{2/\nu}} \right), \quad (2.19)$$

with

$$f = 1 - m(v)z^{2+2/\nu}. \quad (2.20)$$

The metric (2.19) has been written in ingoing Eddington-Finkelstein coordinates (v, r) . The function $m(v)$ in (2.20) defines the thickness of the shell smoothly interpolating between the zero-temperature (2.13) at $v = -\infty$ and black brane backgrounds (2.17) at $v = \infty$.

We choose the following form for the function f

$$f(z, v) = 1 - \frac{M}{2} \left(1 + \tanh \frac{v}{\alpha} \right) z^{\frac{2}{\nu}+2}, \quad (2.21)$$

where α is a parameter. For the calculations in this paper we keep $\alpha = 0.2$.

3 Spatial Wilson loops in a time-independent background

In this work we consider rectangular Wilson loops in the static background (2.13) located in the spatial planes xy_1 (or xy_2) and y_1y_2 . One can delineate the following possible configurations:

- a rectangular loop in the xy_1 (or xy_2) plane with a short side of the length ℓ in the longitudinal x direction and a long side of the length L_{y_1} along the transversal y_1 direction, so that

$$x \in [0, \ell < L_x], \quad y_1 \in [0, L_{y_1}]; \quad (3.1)$$

³The computations have been checked with SageManifolds [45], which is an extension of the free computer algebra system SageMath [46]. The corresponding worksheets are publicly available at the following links:

https://cloud.sagemath.com/3edbca82-97d6-41b3-9b6f-d83ea06fc1e9/raw/Lifshitz_black_brane.html

<https://cloud.sagemath.com/3edbca82-97d6-41b3-9b6f-d83ea06fc1e9/raw/Vaidya-Lifshitz.html>

⁴A more proper terminology would be the Lifshitz-like-Vaidya solution, but we use mainly the Lifshitz-Vaidya for shorter.

- a rectangular loop in the xy_1 plane with a short side of the length ℓ in the transversal y_1 direction and a long side of the length L_x along the longitudinal x direction,

$$x \in [0, L_x], \quad y_1 \in [0, \ell < L_{y_1}]; \quad (3.2)$$

- a rectangular loop in the transversal y_1y_2 plane with a short side of the length ℓ in one of transversal directions (say y_1) and a long side of the length L_{y_2} along the other transversal direction y_2 , namely

$$y_1 \in [0, \ell < L_{y_1}], \quad y_2 \in [0, L_{y_2}]. \quad (3.3)$$

In this section we perform all calculations in the static spacetime (2.17) with (2.18) (using Eddington-Finkelstein coordinates). This background describes holographically the anisotropic media on the boundary with the temperature corresponding to the Hawking temperature of the black brane:

$$T = \frac{1}{\pi} \frac{(\nu + 1)}{2\nu} m^{\frac{\nu}{2\nu+2}}. \quad (3.4)$$

We plot this dependence of the temperature on the mass of the black brane for different values of ν in Fig.1.

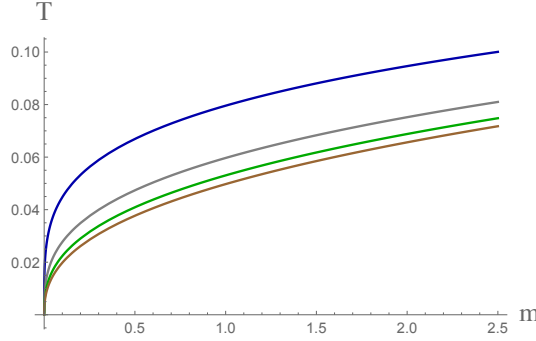


Figure 1. The dependence of the temperature on the black brane mass for $\nu = 1, 2, 3, 4$ (from top to bottom, respectively).

3.1 Wilson loops on the xy_1 -plane

3.1.1 Rectangular strip infinite along the y_1 -direction

We start from the rectangular Wilson loop on the xy_1 -plane with the assumption that it is invariant under the y_1 -direction (see (3.1)). We parameterize the world-sheet of the string in the following way

$$\sigma^1 = x, \quad \sigma^2 = y_1, \quad (3.5)$$

assuming $v = v(x)$, $z = z(x)$ and $z(\pm\ell/2) = 0$.

Taking into account (2.2), (2.19) and (3.5), the Nambu-Goto action can be presented as

$$S_{x, y_1(\infty)} = \int dy_1 dx \frac{1}{z^{1/\nu}} \sqrt{\left(\frac{1}{z^2} - \frac{1}{z^2} f(v')^2 - \frac{2}{z^2} v' z' \right)}, \quad (3.6)$$

where it is supposed $\nu \equiv \frac{d}{dx}$. The subscript $x, y_{1(\infty)}$ in the LHS of (3.6) indicates the orientation of the loop contour. The dynamical system with the action (3.6) has the following integrals of motion

$$\mathcal{J} = -\frac{1}{z^{2+1/\nu}\sqrt{\mathcal{R}}}, \quad (3.7)$$

$$\mathcal{I} = \frac{fv' + z'}{z^{2+1/\nu}\sqrt{\mathcal{R}}}, \quad (3.8)$$

where

$$\mathcal{R} = \frac{1}{z^2} - \frac{1}{z^2}f(z)(v')^2 - \frac{2}{z^2}v'z'. \quad (3.9)$$

The corresponding equation of motion reads

$$z' = \pm \sqrt{f(z) \left(\frac{1}{z^{2+2/\nu}\mathcal{J}^2} - 1 \right) + \left(\frac{\mathcal{I}}{\mathcal{J}} \right)^2}. \quad (3.10)$$

Assuming $\mathcal{I} = 0$ the length ℓ can be defined by

$$\frac{\ell}{2} = \int_{z_0}^{z_*} \frac{dz}{\sqrt{f(z) \left(\left(\frac{z_*}{z} \right)^{2+2/\nu} - 1 \right)}}, \quad (3.11)$$

where z_* is the turning point related with \mathcal{J} as $z_*^{1+1/\nu} = \mathcal{J}^{-1}$. The latter expression can be rewritten in terms of the dimensionless variable $w = z/z_*$ as

$$\ell = 2z_* \int_{z_0/z_*}^1 \frac{w^{1+1/\nu} dw}{\sqrt{f(z_*w)(1 - w^{2+2/\nu})}}. \quad (3.12)$$

By virtue to eq.(3.10) the action (3.6) takes the form

$$S_{x, y_{1(\infty)}} = L_{y_1} \int_{z_0}^{z_*} \frac{1}{z^{1+1/\nu}} \frac{dz}{\sqrt{f(z) \left(1 - \left(\frac{z}{z_*} \right)^{2+2/\nu} \right)}}. \quad (3.13)$$

In terms of w the renormalized Nambu-Goto action (3.13) is represented as

$$S_{x, y_{1(\infty)}, ren} = L_{y_1} \left[\frac{1}{z_*^{1/\nu}} \int_0^1 \frac{dw}{w^{1+1/\nu}} \left[\frac{1}{\sqrt{f(z_*w)(1 - w^{2+2/\nu})}} - 1 \right] - \frac{\nu}{z_*^{1/\nu}} \right]. \quad (3.14)$$

Then pseudopotential $\mathcal{V}_{x, y_{1(\infty)}}$ is given by:

$$\mathcal{V}_{x, y_{1(\infty)}} = \frac{S_{x, y_{1(\infty)}, ren}}{L_{y_1}}. \quad (3.15)$$

In Fig.2 we present the dependence of the pseudopotential $\mathcal{V}_{x, y_{1(\infty)}}$ (3.15) on the length (3.11). We see that for small ℓ the pseudopotential has the Coulomb part deformed by the critical exponent, thus

$$\mathcal{V}_{x, y_{1(\infty)}}(\ell_x, \nu) \underset{\ell_x \sim 0}{\sim} -\frac{\mathcal{C}_1(\nu)}{\ell_x^{1/\nu}}, \quad (3.16)$$

where \mathcal{C}_1 is some constant dependent on ν . Here we put the index x for ℓ to indicate that ℓ_x is the distance along the x -direction. One gets asymptotics (3.16) putting $m = 0$ in (3.11) and (3.14), and taking corrections on m we have for $\nu = 4$

$$\mathcal{V}_{x,y_1(\infty)}(\ell_x, 4) = -\frac{7.80}{\ell_x^{1/4}} \left(1 - 0.012 m \ell_x^{5/2} + \mathcal{O}(m^2 \ell_x^5)\right). \quad (3.17)$$

The asymptotics for arbitrary large ν are presented in Appendix B.

For large distances ℓ_x the pseudopotential $\mathcal{V}_{x,y_1(\infty)}$ behaves as a linearly increasing function

$$\mathcal{V}_{x,y_1(\infty)}(\ell_x, \nu) \underset{\ell \rightarrow \infty}{\sim} \sigma_{s,1}(\nu) \ell_x. \quad (3.18)$$

From dimension arguments one can see $\sigma_{s,1}(\nu) \sim m^{1/2} \sim T^{(1+\nu)/\nu}$.

From Fig.2(d) we also observe that the essential dependence on the anisotropic parameter ν appears with growing values of ℓ . One should be noted that for enough small ℓ the behaviour of $\mathcal{V}_{x,y_1(\infty)}$ extracted from (3.14) for all ν is close to the behaviour of the pseudopotential corresponding to $\nu = 1$ (the AdS case).

3.1.2 Rectangular strip infinite along the x -direction

Another possible configuration in the xy_1 plane is the rectangular Wilson loop whose contour is infinite along the x -direction and has a finite size along the y_1 -direction (see (3.2)). We specify this type of the configuration by the subscript $y_1, x_{(\infty)}$. For the parameterization (3.5) we take $v = v(y_1)$, $z = z(y_1)$ with boundary conditions $z(\pm\ell/2) = 0$. By virtue to this assumption the Nambu-Goto action (2.2) reads

$$S_{y_1, x_{(\infty)}} = \int dy_1 dx \frac{1}{z} \sqrt{\left(\frac{1}{z^{2/\nu}} - \frac{1}{z^2} f(v')^2 - \frac{2}{z^2} v' z'\right)}, \quad (3.19)$$

where it is supposed $\iota \equiv \frac{d}{dy_1}$.

The integrals of motion corresponding to the action (3.19) are

$$\mathcal{J} = -\frac{1}{z^{1+2/\nu} \sqrt{\mathcal{R}}}, \quad (3.20)$$

$$\mathcal{I} = \frac{f v' + z'}{z^3 \sqrt{\mathcal{R}}}, \quad (3.21)$$

with

$$\mathcal{R} = \frac{1}{z^{2/\nu}} - \frac{1}{z^2} f(z, v)(v')^2 - \frac{2}{z^2} v' z'. \quad (3.22)$$

The equation of motion for the system governed by (3.19) is given by

$$z' = \pm z^{1-1/\nu} \sqrt{f(z) \left(\frac{1}{z^{2+2/\nu} \mathcal{J}^2} - 1\right) + \left(\frac{\mathcal{I}}{\mathcal{J}}\right)^2 z^{2-2/\nu}}. \quad (3.23)$$

Under assumption $\mathcal{I} = 0$ the expression for the length can be written down in terms of the w -variable

$$\ell = 2z_*^{1/\nu} \int_0^1 \frac{w^{2/\nu} dw}{\sqrt{f(z_* w) (1 - w^{2+2/\nu})}}, \quad (3.24)$$

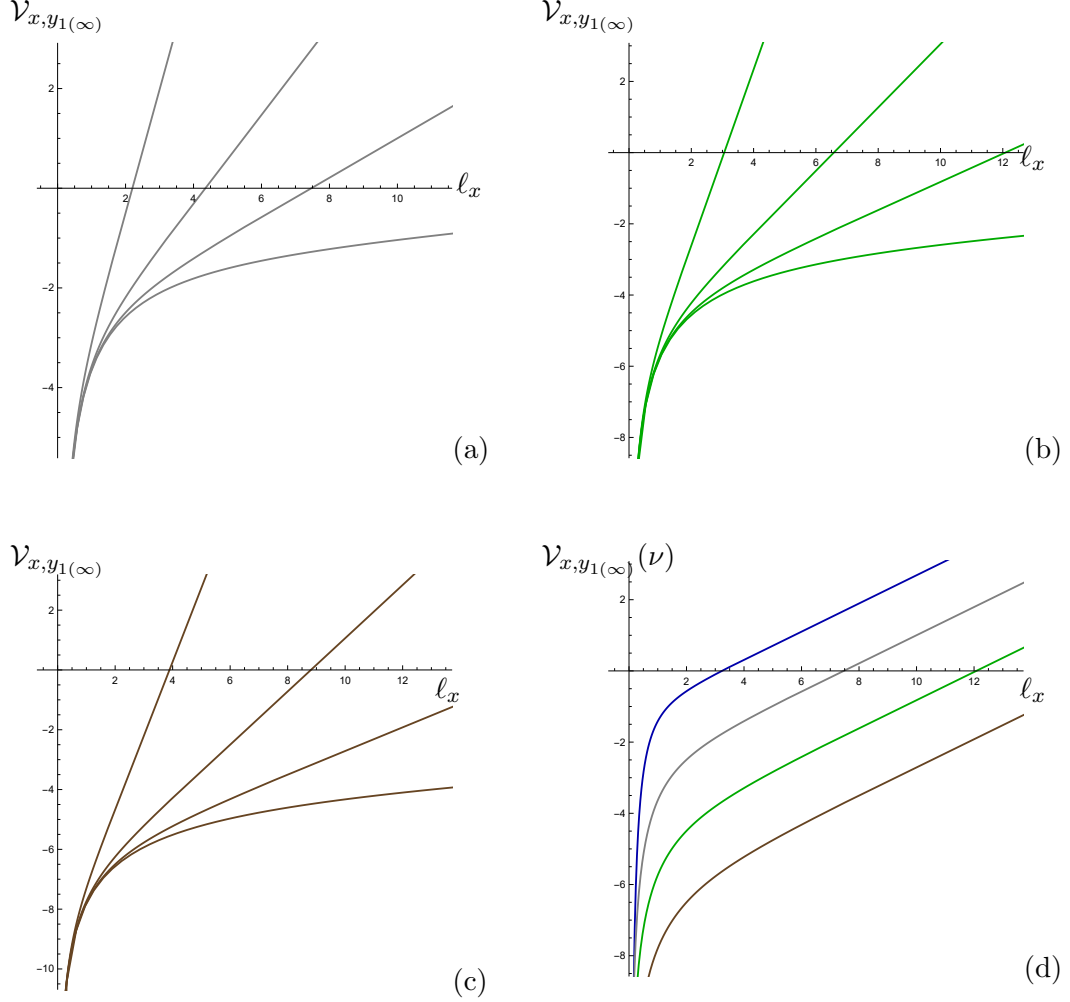


Figure 2. The pseudopotential $\mathcal{V}_{x,y_1(\infty)}$ corresponding to the action $S_{x,y_1(\infty)}$ (3.14) as a function of ℓ (3.11), $\nu = 2, 3, 4$ ((a),(b),(c) respectively). We take the temperature $T = 0.08, 0.2, 0.3, 0.5$ (from down to top) for all (a), (b) and (c). In (d): the behavior of the pseudopotential corresponding to (3.14) for $\nu = 1, 2, 3, 4$ (from top to down) at $T = 0.2$.

where the turning point z_* is related to \mathcal{J} as $z_*^{1+1/\nu} = \mathcal{J}^{-1}$.

The renormalized Nambu-Goto action (3.24) reads

$$S_{y_1, x(\infty), ren} = L_x \left[\frac{1}{z_*} \int_{z_0/z_*}^1 \frac{dw}{w^2} \left[\frac{1}{\sqrt{f(z_*w) (1 - w^{2+2/\nu})}} - 1 \right] - \frac{1}{z_*} \right], \quad (3.25)$$

while the pseudopotential $\mathcal{V}_{y_1, x(\infty)}$ related to (3.25) is:

$$\mathcal{V}_{y_1, x(\infty)} = \frac{S_{y_1, x(\infty), ren}}{L_x}. \quad (3.26)$$

In Fig. 3 we show the dependence of the pseudopotential extracted from the action (3.25) on the length ℓ for different values of the temperature and the dynamical exponent. Now the pseudopotential has a power-law dependence on ν for small ℓ , so that

$$\mathcal{V}_{y_1, x(\infty)} \underset{\ell_y \rightarrow 0}{\sim} -\frac{\mathcal{C}_2(\nu)}{\ell_y^\nu}, \quad (3.27)$$

with some constant \mathcal{C}_2 dependent on ν . Here we put the index y for ℓ to indicate that ℓ_y is the distance along the y -direction. One gets asymptotics (3.27) with $m = 0$ in (3.24) and (3.25), and taking corrections on m we obtain for $\nu = 4$

$$\mathcal{V}_{y_1, x(\infty)} = -\frac{13.5}{\ell_y^4} (1 - 0.00031 m \ell_y^{10} + \mathcal{O}(m^2 \ell_y^{20})). \quad (3.28)$$

However, for large distances the pseudopotential represents a linear function of ℓ again

$$\mathcal{V}_{y_1, x(\infty)}(\ell_y, \nu) \underset{\ell \rightarrow \infty}{\sim} \sigma_{s,2}(\nu) \ell_y. \quad (3.29)$$

and by dimensional analysis $\sigma_{s,2}(\nu) \sim m^{\frac{1}{2}} \sim T^{(1+\nu)/\nu}$.

From Fig. 3(d) we also see that the dependence of $\mathcal{V}_{y_1, x(\infty)}(\ell, \nu)$ on the dynamical exponent ν disappears at large ℓ and the pseudopotential $\mathcal{V}_{y_1, x(\infty)}(\ell, \nu)$ for all ν are linear growing functions slightly deviating from the *AdS* case ($\nu = 1$).

3.2 Wilson loop on the $y_1 y_2$ -plane

Now we come to the spatial rectangular Wilson loop located on the $y_1 y_2$ -plane. Let us assume that the loop contour is infinite along the y_2 -direction and has the finite extent of the length ℓ in the y_1 -direction (see (3.3)). We specify this type of the orientation by the subscript $y_1, y_2(\infty)$, choosing only transversal coordinates for the parameterization of the worldsheet

$$\sigma^1 = y_1, \quad \sigma^2 = y_2. \quad (3.30)$$

Taking into account, that $z = z(y_1)$ satisfying $z(\pm\ell/2)$ one can represent the string action (2.2) in the following form

$$S_{y_1, y_2(\infty)} = \int dy_1 dy_2 \frac{1}{z^{1/\nu}} \sqrt{\left(\frac{1}{z^{2/\nu}} - \frac{1}{z^2} f(v')^2 - \frac{2}{z^2} v' z' \right)}, \quad (3.31)$$

where it is supposed $\prime \equiv \frac{d}{dy_1}$. The integrals of motion are

$$\mathcal{J} = -\frac{1}{z^{3/\nu} \sqrt{\mathcal{R}}}, \quad (3.32)$$

$$\mathcal{I} = \frac{f v' + z'}{z^{2+1/\nu} \sqrt{\mathcal{R}}}, \quad (3.33)$$

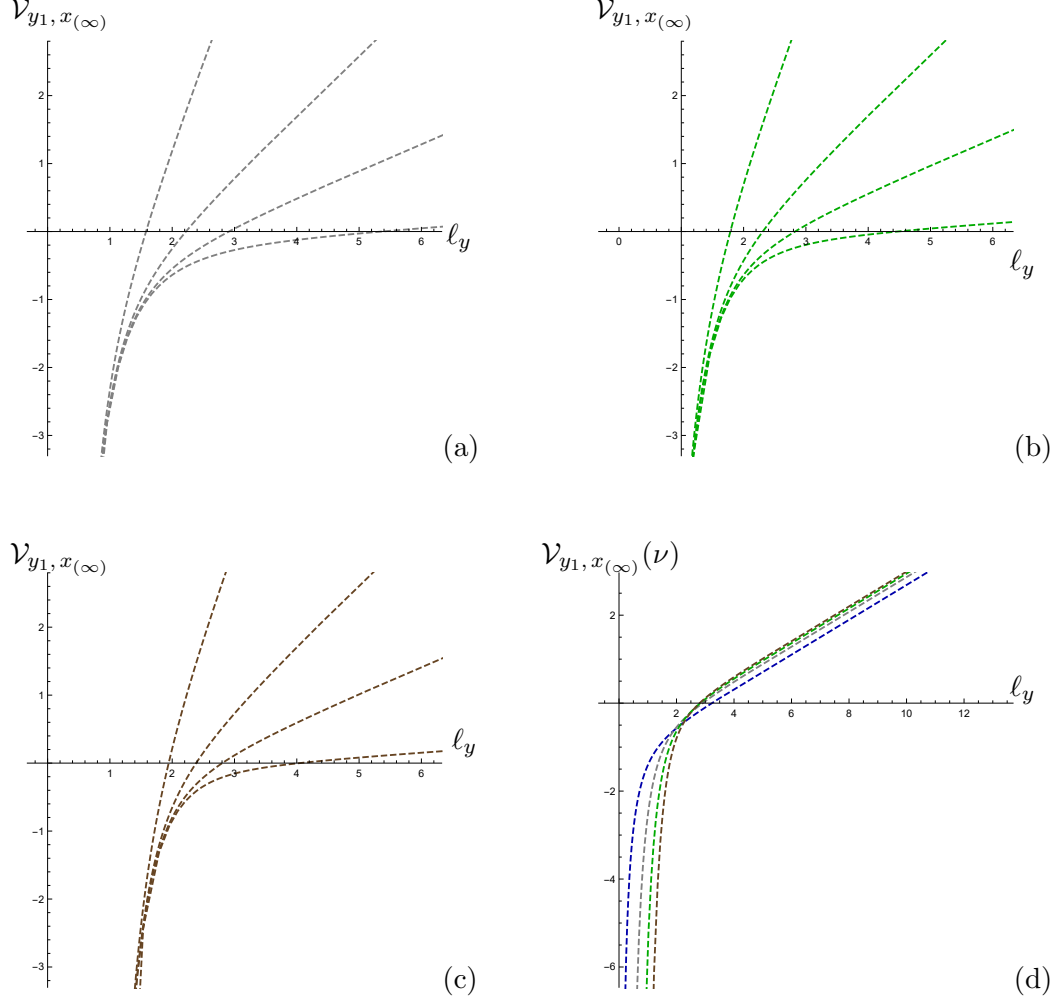


Figure 3. The pseudopotential $\mathcal{V}_{y1, x(\infty)}$ extracted from action (3.25) as a function of ℓ for $\nu = 2, 3, 4$ ((a),(b),(c), respectively). We take $T = 0.08, 0.2, 0.3, 0.5$ from down to top, respectively, for (a),(b) and (c). In (d) we plot the behaviour of \mathcal{V} corresponding to (3.25) for $\nu = 1, 2, 3, 4$ (from left to right, respectively) at $T = 0.2$.

where we denote

$$\mathcal{R} = \frac{1}{z^{2/\nu}} - \frac{1}{z^2} f(z, v) (v')^2 - \frac{2}{z^2} v' z'. \quad (3.34)$$

The equation of motion corresponding to (3.31) reads

$$z' = \pm z^{1-1/\nu} \sqrt{f(z) \left(\frac{1}{z^{4/\nu} \mathcal{J}^2} - 1 \right) + \left(\frac{\mathcal{I}}{\mathcal{J}} \right)^2 z^{2-2/\nu}}. \quad (3.35)$$

Putting $\mathcal{I} = 0$ one gets the following relation for the length in terms of the w -variable

$$\ell = z_*^{1/\nu} \int \frac{dw}{w^{1-3/\nu} \sqrt{f(z_* w) (1 - w^{4/\nu})}}, \quad (3.36)$$

where z_* is the turning point related to \mathcal{J} as $z^2/\nu = \mathcal{J}^{-1}$.

Finally, the renormalized action (3.31) takes the form

$$S_{y_1, y_2(\infty), ren} = L_{y_2} \left(\frac{1}{z_*^{1/\nu}} \int_{z_0/z_*}^1 \frac{dw}{w^{1+1/\nu}} \left[\frac{1}{\sqrt{f(z_* w) (1 - w^{4/\nu})}} - 1 \right] - \frac{\nu}{z_*^{1/\nu}} \right). \quad (3.37)$$

The pseudopotential $\mathcal{V}_{y_1, y_2(\infty)}$ extracted from (3.37) reads as:

$$\mathcal{V}_{y_1, y_2(\infty)} = \frac{S_{y_1, y_2(\infty)}}{L_{y_2}}. \quad (3.38)$$

In Fig.4 we display the behaviour of the pseudopotential (3.38) on the length (3.36).

It is easy to see that the behavior of $\mathcal{V}_{y_1, y_2(\infty)}$ in Fig.4 is rather different from two previous cases. From Fig.4 (d) we observe, that now the dependence on ν is driven by some constant \mathcal{C}_3 relying on ν . It should be noted that the pseudopotentials strongly deviate from the AdS case ($\nu = 1$) both in the UV and the IR regions of ℓ . Thus, one can write for small ℓ

$$\mathcal{V}_{y_1, y_2(\infty)}(\ell_y, \nu) \underset{\ell \rightarrow 0}{\sim} -\frac{\mathcal{C}_3(\nu)}{\ell_y}, \quad (3.39)$$

where \mathcal{C}_3 is some constant dependent on ν . For $\nu = 4$ one can write down (3.39) with the corrections on m in the following form

$$\mathcal{V}_{y_1, y_2(\infty)}(\ell_y, 4) = -\frac{23.0}{\ell_y} (1 - 0.741 \cdot 10^{-9} m \ell_y^{10} + \mathcal{O}(m^2 \ell_y^{20})). \quad (3.40)$$

For large ℓ we have

$$\mathcal{V}_{y_1, y_2(\infty)}(\ell_y, \nu) \underset{\ell_y \rightarrow \infty}{\sim} \sigma_{s,3}(\nu) \ell_y \quad (3.41)$$

and by dimensional analysis $\sigma_{s,3}(\nu) \sim m^{\frac{1}{1+\nu}} \sim T^{2/\nu}$.

3.3 Spatial string tension dependence on the orientation

It is interesting to analyze the behavior of the spatial string tension σ_s (2.8) for different orientations of the Wilson loop, i.e. the behaviour of $\sigma_{s,i}$, $i = 1, 2, 3$ given by (3.18), (3.29) and (3.41). The temperature dependences of the spatial string tension in the confining background, which reproduces the Cornell potential [13], and the deconfining one have been studied in [71] and [72], respectively. In [73] the universal behaviour of the spatial string tension for multiquark configurations was found. In the AdS/QCD model [13] the string tension dependence matching lattice data was found in [70]. In Fig.5 (the left panel) we present the dependence of the spatial string tension $\sqrt{\sigma_s}$ as a function of T for all cases of

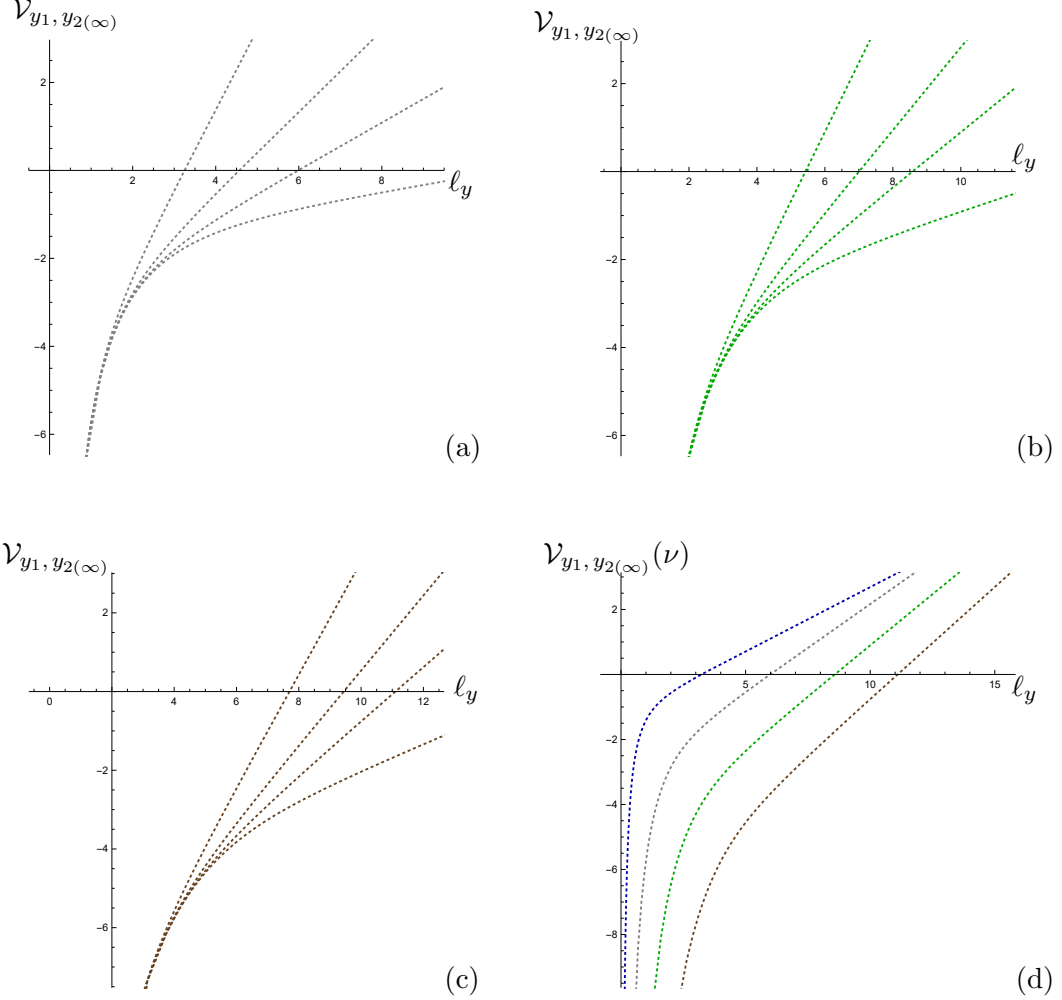


Figure 4. The pseudopotential $\mathcal{V}_{y1, y2(\infty)}$ extracted from $S_{y1, x(\infty)}$ (3.37) as a function of ℓ for $\nu = 2, 3, 4$ ((a),(b),(c), respectively). We take $T = 0.08, 0.2, 0.3, 0.5$ from down to top, respectively, for (a),(b) and (c). In (d) we plot the behaviour of \mathcal{V} corresponding to (3.37) for $\nu = 1, 2, 3, 4$ (from left to right) at $T = 0.2$.

the orientation and for $\nu = 1, 2, 3, 4$. We see, that for the configurations located on the xy_1 -plane (partially longitudinal orientations shown by solid and dashed lines) the temperature dependence of the string tension for different ν are rather similar. The deviations of solid lines from dashed ones increase with increasing T . We also see that the string tension corresponding to the Wilson loop in the y_1y_2 -plane (the totally transversal orientation shown by the dotted lines) differs from the behaviour of the Wilson loop including the longitudinal direction, showing less dependence on the temperature with increasing ν . All

these plots indicate that the structure of magnetic fields in our holographic model has strong dependence on its orientation. In the right panel of Fig.5 the spatial string tension $\sqrt{\sigma_s}$ for different orientations for $\nu = 4$ is presented.

We note that the behaviour of magnetic Wilson loops in heavy ion collisions was worked out in [74, 75] and is put in the context of the color glass condensate model. The universal behavior of a large magnetic Wilson loop was found to have a nontrivial power-law dependence on the loop area. They have also argued that in contrast to usual Coulomb phase behaviour, magnetic flux does not propagate uniformly in the transverse plane, but instead, it is concentrated in small domains. In our work the Coulomb phases of pseudopotentials are modified for orientations different from the transversal one.

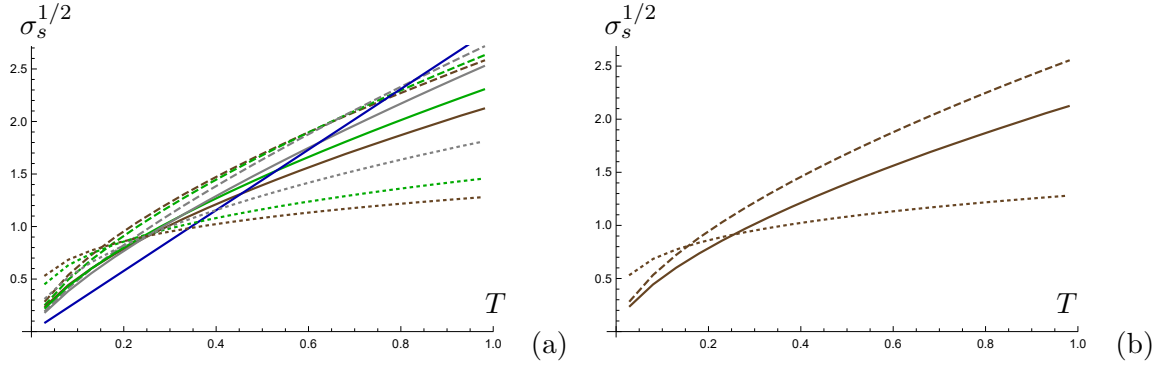


Figure 5. The dependence of the spatial string tension $\sqrt{\sigma_s}$ on orientation and temperature. The solid lines corresponds to the rectangular Wilson loop with a short extent in the x -direction, while the dashed lines correspond to a short extent in the y -direction. The dotted lines correspond to the rectangular Wilson loop in the transversal $y_1 y_2$ -plane. (a) Blue line corresponds to $\nu = 1$, gray lines correspond to $\nu = 2$, green lines correspond to $\nu = 3$ and the brown ones correspond to $\nu = 4$. (b) The spatial string tension $\sqrt{\sigma_s}$ for different orientations for $\nu = 4$.

4 Spatial Wilson loops in a time-dependent background

Now we move to consider the thermalization of rectangular Wilson loops in the Lifshitz-Vaidya background (2.19)-(2.21), which describes collapsing geometry in the Lifshitz-like spacetime. We proceed in a similar manner as in the static case studying three possible configurations of spatial Wilson loops.

4.1 Wilson loops on the xy_1 -plane

4.1.1 Rectangular strip infinite along the y_1 -direction

As in Sec. 3 we start from the spatial rectangular Wilson loop on the xy_1 -plane with the assumption that one side is infinite along the y_1 -direction and has finite size along the x -direction (see (3.1)). Here we suppose the dependence $v = v(x)$, $z = z(x)$. The Nambu-Goto action takes the form similar to (3.6)

$$S_{x,y_1(\infty)} = L_y \int \frac{dx}{z^{1+1/\nu}} \sqrt{1 - f(z, v)v'^2 - 2v'z'}, \quad (4.1)$$

where we define $' \equiv \frac{d}{dx}$.

The corresponding equations of motion are

$$v'' = \frac{1}{2} \frac{\partial f}{\partial z} v'^2 + \frac{(\nu+1)}{\nu z} (1 - f v'^2 - 2v'z'), \quad (4.2)$$

$$z'' = -\frac{\nu+1}{\nu} \frac{f}{z} + \frac{\nu+1}{\nu} \frac{f^2 v'^2}{z} - \frac{1}{2} \frac{\partial f}{\partial v} v'^2 - \frac{1}{2} f v'^2 \frac{\partial f}{\partial z} - v' z' \frac{\partial f}{\partial z} + 2 \frac{(\nu+1)}{\nu z} f v' z', \quad (4.3)$$

which coincide with the equations for the AdS case for $\nu = 1$.

Eqs.(4.2)-(4.3) obey the following boundary conditions

$$z(\pm\ell) = 0, \quad v(\pm\ell) = t, \quad (4.4)$$

where ℓ is the length of the Wilson loop along the x -direction.

To solve numerically the equations of motion (4.2)-(4.3) with (4.4) we impose the following initial conditions

$$z(0) = z_*, \quad v(0) = v_*, \quad (4.5)$$

$$z'(0) = 0, \quad v'(0) = 0. \quad (4.6)$$

Figure 6 shows the typical behaviour of the solutions to eqs.(4.2)-(4.3) that satisfy the boundary conditions (4.4) for different values of the critical exponent ν . In these pictures we observe the evolution of string profiles during the formation of the black brane horizon by the infalling shell at $z = 1$.

Given a solution $(v(x), z(x))$ to eqs.(4.2)-(4.3) one can compute the functional for the Nambu-Goto action (4.1).

We note that the dynamical system governed by (4.1) has the following integral of motion

$$\mathcal{J} = -\frac{1}{z^{1+1/\nu} \sqrt{\mathcal{R}}}, \quad (4.7)$$

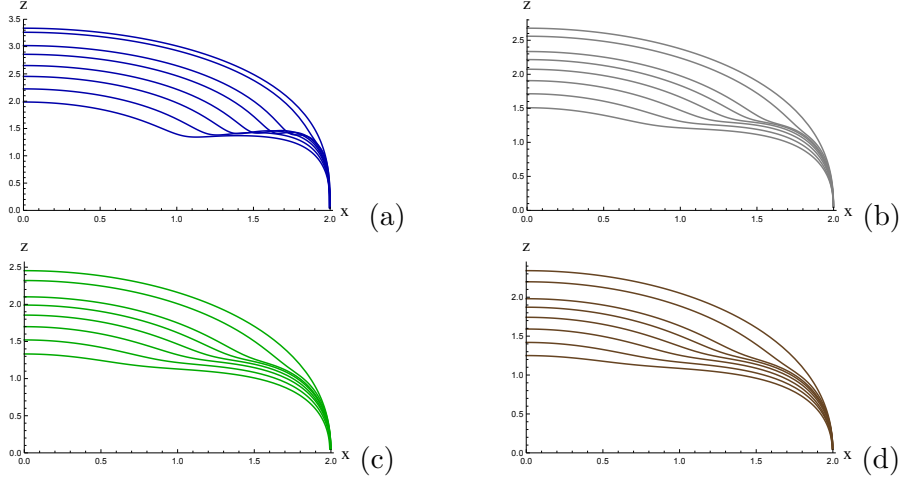


Figure 6. Profiles of the string $z(x)$, $z(2) = 0$ at different moments of the boundary time $\nu = 1, 2, 3, 4$ ((a),(b),(c),(d), respectively). In (2.21) we take $M = 1$.

where we denote

$$\mathcal{R} = 1 - f v'^2 - 2v' z'. \quad (4.8)$$

Taking into account (4.7)-(4.8) one can represent (4.1) in the following form

$$S_{x,y_1(\infty)} = L_y \int_0^{l_x - \epsilon} \frac{dx}{z^{1+1/\nu}} \left(\frac{z_*}{z} \right)^{1+1/\nu}, \quad (4.9)$$

where z_* is the turning point defined from the requirements $z' = v' = 0$ and related with \mathcal{J} as $z_*^{1/\nu+1} = \mathcal{J}^{-1}$.

Coming to integration with respect to the z -variable the latter renormalized expression can be represented as

$$S_{x,y_1(\infty),ren} = -L_{y_1} \left(\int_{z_0}^{z_*} \frac{[\mathbf{b}(z) - \mathbf{b}(z_0)]}{z^{1+1/\nu}} dz - \nu \frac{\mathbf{b}(z_0)}{z_*^{1/\nu}} \right), \quad (4.10)$$

with the pseudopotential expressed as :

$$\mathcal{V}_{x,y_1(\infty)} = \frac{S_{x,y_1(\infty),ren}}{L_{y_1}}. \quad (4.11)$$

In (4.10) we have introduced the quantity \mathbf{b} defined by

$$\mathbf{b}(z) = \frac{1}{z'} \left(\frac{z_*}{z} \right)^{1+1/\nu}. \quad (4.12)$$

We study the behaviour of the function (4.12) on the solution to eqs.(4.2)-(4.3) in Appendix A.1. From Fig. 16 we observe that $\mathbf{b}(z)$ tends to be -1 for $z \rightarrow 0$. Thus, the renormalization is similar to the static configuration, since the UV divergence is similar to that one in the shell free case.

In Fig. 7 we present the behaviour of the renormalized pseudopotential $\mathcal{V}_{x,y_1(\infty)}$ derived from the action (4.10) as a function of ℓ at fixed time moments for different values of ν .

We see that for small distances the pseudopotential behaves similarly for different values of t . This dependence strengthens with increasing ν . Thus, one can conclude during the thermalization process the potential asymptotes to thermal equilibrium for large t .

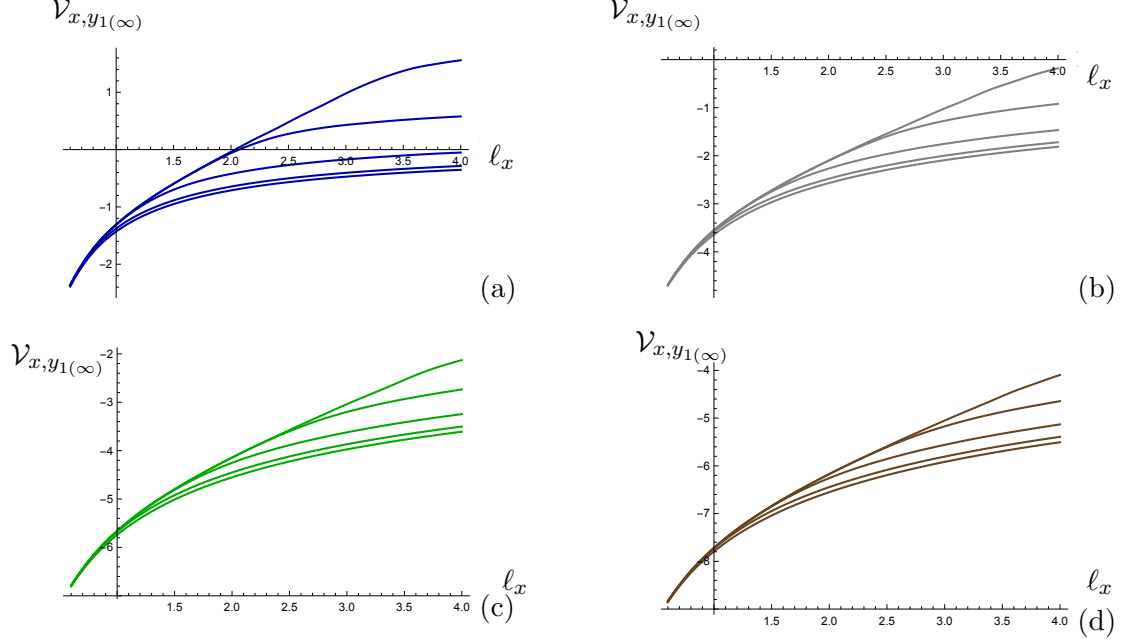


Figure 7. The pseudopotential $\mathcal{V}_{x,y_1(\infty)}$ as a function of ℓ at fixed values of t for $\nu = 1, 2, 3, 4$ ((a),(b),(c),(d), respectively). Different curves correspond to time $t = 0.1, 0.5, 0.9, 1.4, 2$ (from down to top, respectively). In (2.21) we take $M = 1$.

It is also instructive to follow the evolution of the quantity $\delta\mathcal{V}_{x,y_1(\infty)}(\ell_x, t)$ defined by

$$\delta\mathcal{V}_{x,y_1(\infty)}(\ell_x, t) = \mathcal{V}_{x,y_1(\infty)}(\ell_x, t) - \mathcal{V}_{x,y_1(\infty)}(\ell_x, t_f), \quad (4.13)$$

where $\mathcal{V}_{x,y_1(\infty)}(\ell_x, t)$ is the pseudopotential at the current time and $\mathcal{V}_{x,y_1(\infty)}(\ell_x, t_f)$ is the pseudopotential at the moment of time when the black brane has already been formed. In Fig.8 the results of our numerical studies of (4.13) are shown. We plot this quantity (with the negative sign) for different values of ℓ and ν . From Fig. 8 it is seen the pseudopotential reaches saturation and then flattens out for enough large size of the strip. The value of the saturation time grows with increasing ℓ for all values of ν . At the same time, the saturation is reached faster for large ν .

4.1.2 Rectangular strip infinite along the x -direction

Now we consider the rectangular Wilson loop on the xy_1 -plane with the assumption that its contour is infinite along the x -direction while it has finite stretch along the y_1 -direction (see (3.2)). As in the previous section, we specify this type of the strip by the subscript

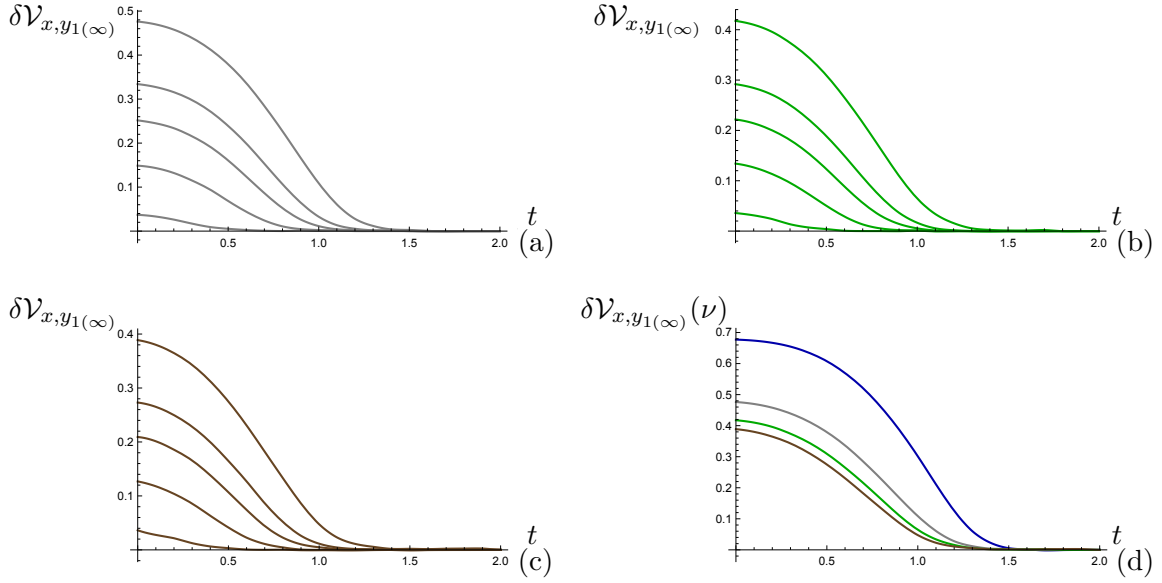


Figure 8. The time dependence of the quantity $-\delta\mathcal{V}_{x,y_1(\infty)}(\ell_x,t)$, given by (4.13), for different values of the length ℓ , $\nu = 2, 3, 4$ ((a),(b),(c), respectively). Different curves correspond to $\ell = 0.7, 1.2, 1.5, 1.7, 2$ (from down to top, respectively). In (d) we have shown the quantity $-\delta\mathcal{V}_{x,y_1(\infty)}(\ell_x,t)$ as a function of t at $\ell = 2$ for $\nu = 1, 2, 3, 4$ (from top to down, respectively). In (2.21) we take $M = 1$.

$y_1, x_{(\infty)}$. Thus, the corresponding Nambu-Goto action can be represented by

$$S_{y_1, x_{(\infty)}} = L_x \int dy_1 \frac{1}{z^2} \sqrt{\left(\frac{1}{z^{2/\nu-2}} - f(z, v)(v')^2 - 2v'z' \right)}, \quad (4.14)$$

with the notation $\iota \equiv \frac{d}{dy_1}$. The time-independent analogue of (4.14) is given by (3.19).

The equations of motion following from (4.14) are

$$v'' = \frac{1}{2} \frac{\partial f}{\partial z} v'^2 + \frac{\nu+1}{\nu z} \left(z^{2-2/\nu} - \frac{2\nu}{(1+\nu)} f v'^2 - 2v'z' \right), \quad (4.15)$$

$$z'' = -\frac{\nu+1}{\nu} f z^{1-2/\nu} + \frac{2(\nu-1)z'^2}{\nu} + \frac{2f^2 v'^2}{\nu z} - \frac{1}{2\nu} \frac{\partial f}{\partial v} v'^2 - \frac{1}{2\nu} f \frac{\partial f}{\partial z} v'^2 - z'v' \frac{\partial f}{\partial z} + \frac{4}{z} f z'v'. \quad (4.16)$$

It is worth to be noted that eqs.(4.15)-(4.16) match with (4.2)-(4.3) taken with $\nu = 1$ and also reproduce those for the AdS-case.

The boundary conditions for eqs.(4.15)-(4.16) read

$$z(\pm l) = 0, \quad v(\pm l) = t, \quad (4.17)$$

where ℓ is the length of the Wilson loop along the y_1 -direction.

The numerical solutions to (4.15)-(4.16) with (4.17) for different values of ν and a brief discussion are presented in Appendix A.2.

The integral of motion corresponding to (4.14) is

$$\mathcal{J} = -\frac{1}{z^{2/\nu}\sqrt{\mathcal{R}}}, \quad (4.18)$$

where

$$\mathcal{R} = \frac{1}{z^{2/\nu-2}} - f v'^2 - 2v'z'. \quad (4.19)$$

Taking into account (4.18)-(4.19) the action (4.14) is represented in the form

$$S_{y_1, x(\infty)} = L_x \int_0^{l_x - \epsilon} dx \frac{z_*^{1/\nu+1}}{z^{2/\nu+2}}, \quad (4.20)$$

with the turning point z_* defined from the requirements $z' = v' = 0$ and related with \mathcal{J} as $z_*^{1/\nu+1} = \mathcal{J}^{-1}$.

As in the previous case we compute the functional (4.20) on the solutions to eqs.(4.15)-(4.16).

In the z -variable the renormalized Nambu-Goto action (4.20) can be written down as

$$S_{y_1, x(\infty), ren} = -L_x \int_0^{z_*} \frac{\mathbf{b}(z) - \mathbf{b}(z_0)}{z^2} dz - \frac{\mathbf{b}(z_0)}{z_*}, \quad (4.21)$$

with \mathbf{b} defined by

$$\mathbf{b}(z) = \frac{1}{z'} \left(\frac{z_*^{1+1/\nu}}{z^{2/\nu}} \right). \quad (4.22)$$

We also present plots of the behaviour of $\mathbf{b}(z)$ (4.22) in Appendix A.2. The pseudopotential is expressed from the action (4.21) as:

$$\mathcal{V}_{y_1, x(\infty)} = \frac{S_{y_1, x(\infty), ren}}{L_{y_1}}. \quad (4.23)$$

The renormalized pseudopotential derived from the action (4.21) as a function of ℓ for different values of t and ν is demonstrated in Fig. 9. Here we again observe that for small ℓ the behavior of the pseudopotential is similar for different values of t . So, the pseudopotential \mathcal{V} is evolved approaching the thermal equilibrium for late times. As in the previous case the behavior intensifies with the increasing value of the dynamical exponent.

To probe the thermalization of the Wilson loops we also define the quantity

$$\delta\mathcal{V}_{y_1, x(\infty)}(\ell_y, t) = \mathcal{V}_{y_1, x(\infty)}(\ell_y, t) - \mathcal{V}_{y_1, x(\infty)}(\ell_y, t_f), \quad (4.24)$$

where $\mathcal{V}_{y_1, x(\infty)}(\ell_y, t)$ is the pseudopotential extracted from the action (4.21) at the current time and $\mathcal{V}_{y_1, x(\infty)}(\ell_y, t_f)$ is the pseudopotential at the time when the black brane has already formed. In Fig. 10 we plot (4.24), taken with the negative sign, as a function

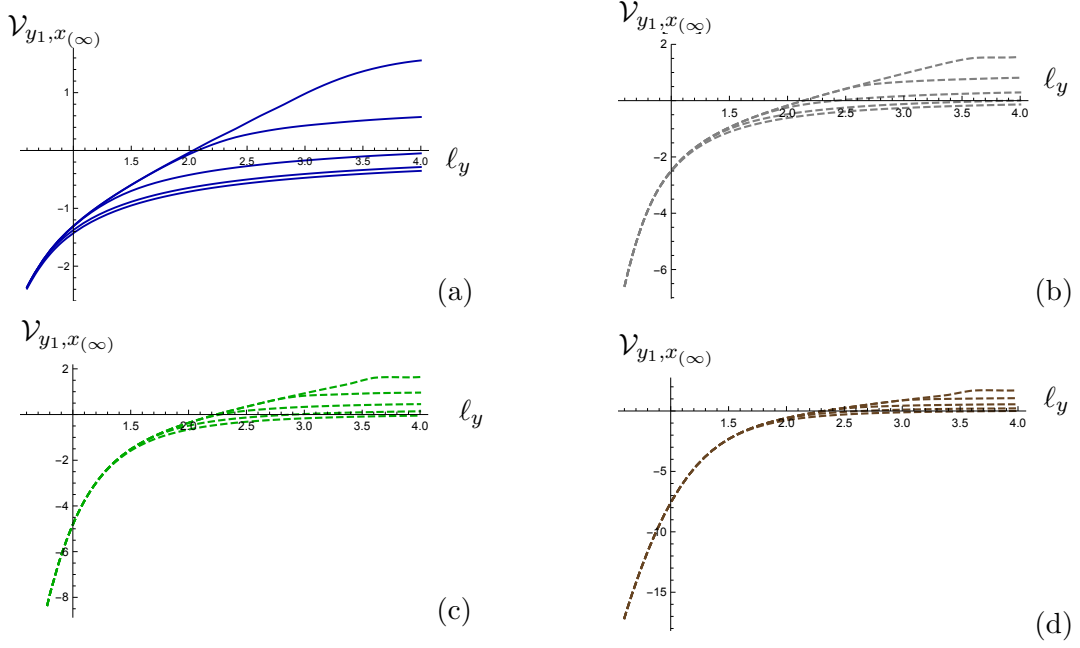


Figure 9. The pseudopotential $\mathcal{V}_{y_1, x(\infty)}$ as a function of ℓ at fixed values of t for $\nu = 1, 2, 3, 4$ ((a),(b),(c),(d), respectively). Different curves correspond to $t = 0.1, 0.5, 0.9, 1.4, 2$ from down to top. In (2.21) we take $M = 1$.

of t at fixed values of ℓ . From Fig. 10 we see that for small ℓ the saturation value is achieved for a shorter period of time than for large distances. Here we also observe that the thermalization process of the Wilson loops depends on the dynamical exponent. This is in contrast to the previous case there is no substantial dependence, on a given scale, of the thermalization time on the dynamical exponent.

Comparing Fig.8 and Fig.10 one can see that for the same scale ℓ the thermalization of the Wilson loop occurs faster for the configuration with a long extent in the y_1 -direction. The dependence on the dynamical exponent ν is also stronger for the latter case of the orientation.

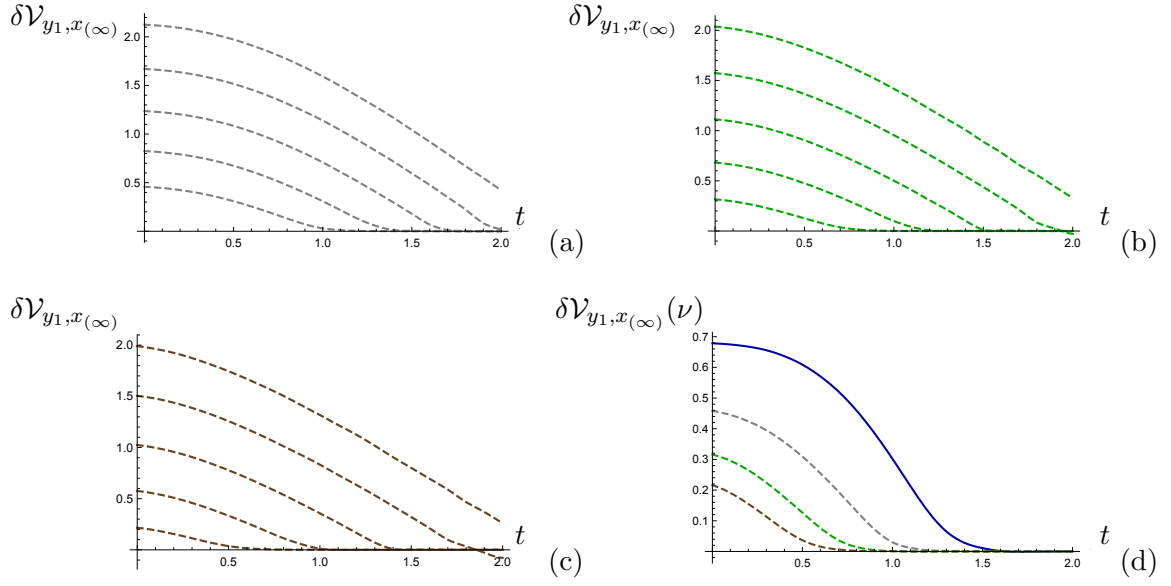


Figure 10. The time dependence of $-\delta\mathcal{V}_{y_1, x(\infty)}(\ell_y, t)$, defined by (4.24), for different values of the length ℓ , $\nu = 2, 3, 4$ ((a),(b),(c), respectively). Different curves correspond to $\ell = 2, 2.5, 3, 3.5, 4$ (from down to top, respectively). In (d) we have shown the quantity $-\delta\mathcal{V}_2(\ell_y, t)$ as a function of t at $\ell = 2$ for $\nu = 1, 2, 3, 4$ (from top to down, respectively). In (2.21) we take $M = 1$.

4.2 Wilson loop on the $y_1 y_2$ -plane

Finally, we come to the configuration located on the $y_1 y_2$ -plane. We assume that this infinite rectangular strip is invariant along the y_2 -direction, see (3.3). As in Sect. 3.2 we use $y_1, y_{2,(\infty)}$ for the subscript of the action.

$$S_{y_1, y_{2,(\infty)}} = L_{y_2} \int dy_1 \frac{1}{z^{1+1/\nu}} \sqrt{\left(\frac{1}{z^{2/\nu-2}} - f(v')^2 - 2v'z' \right)}, \quad (4.25)$$

where we define $\iota \equiv \frac{d}{dy_1}$.

The equations of motion corresponding to (4.25) can be written down in the following form

$$v'' = \frac{1}{2} \frac{\partial f}{\partial z} v'^2 + \frac{2}{z\nu} \left(z^{2-2/\nu} - \frac{\nu+1}{2} f v'^2 - 2v'z' \right), \quad (4.26)$$

$$\begin{aligned} z'' = & -\frac{2}{\nu} f z^{1-2/\nu} + 2 \frac{\nu-1}{\nu} \frac{z'^2}{z} + \frac{\nu+1}{\nu z} f^2 v'^2 - \frac{1}{2} \frac{\partial f}{\partial v} v'^2 - \frac{1}{2} f \frac{\partial f}{\partial z} v'^2 \\ & - z' v' \frac{\partial f}{\partial z} + \frac{2(\nu+1)}{\nu z} f v' z'. \end{aligned} \quad (4.27)$$

One can check that eqs. (4.26)-(4.27) coincide with (4.2)-(4.3) and (4.15)-(4.16) for $\nu = 1$ as well as come to be the equations for the AdS case.

The boundary conditions to be satisfied by eqs.(4.26)-(4.27) have the standard form

$$z(\pm\ell) = 0, \quad v(\pm\ell) = t, \quad (4.28)$$

where ℓ is the length of the Wilson loop along the y_1 -direction. We show the numerical solutions to (4.26)-(4.27) for different values of ν in Fig. 19 in Appendix A.3.

The integral of motion for the configuration governed by the action (4.25) reads

$$\mathcal{J} = -\frac{1}{z^{\frac{3}{\nu}-1}\sqrt{\mathcal{R}}}, \quad (4.29)$$

where we define

$$\mathcal{R} = \frac{1}{z^{2/\nu-2}} - f(v')^2 - 2v'z'. \quad (4.30)$$

Following our strategy we compute the functional (4.25) on a given solution to (4.26)-(4.27).

Plugging (4.29) into (4.25) we come to the following form for the functional of the Nambu-Goto action

$$S_{y_1, y_2, (\infty)} = L_{y_2} \int_0^{l-\epsilon} dy_1 \frac{z_*^{2/\nu}}{z^{4/\nu}}, \quad (4.31)$$

where the turning point z_* is related with \mathcal{J} as $z_*^{2/\nu} = \mathcal{J}^{-1}$. The renormalized action in terms of the z -variable reads

$$S_{y_1, y_2, (\infty), ren} = -L_{y_2} \left(\int_{z_0}^{z_*} \frac{[\mathfrak{b}(z) - \mathfrak{b}(z_0)]}{z^{1+1/\nu}} dz - \nu \frac{\mathfrak{b}(z_0)}{z_*^{1/\nu}} \right), \quad (4.32)$$

where we introduce the function \mathfrak{b} defined by

$$\mathfrak{b}(z) = \frac{1}{z'} \left(\frac{z_*^{2/\nu}}{z^{3/\nu-1}} \right). \quad (4.33)$$

Here the pseudopotential is expressed from (4.32) as:

$$\mathcal{V}_{y_1, y_2(\infty)} = \frac{S_{y_1, y_2(\infty), ren}}{L_{y_2}} \quad (4.34)$$

In Appendix A.3 in Fig. 20 we display the behaviour of the function $\mathfrak{b}(z)$ given by (4.33) as a function of z for different values of ν .

The dependence of the pseudopotential $\mathcal{V}_{y_1, y_2(\infty)}$ on the length ℓ is shown in Fig.11. As for the previous configurations of Wilson loop located on the xy_1 -plane, the pseudopotential $\mathcal{V}_{y_1, y_2(\infty)}$ tends to its thermal value for large t .

We also compute numerically the quantity

$$\delta\mathcal{V}_{y_1, y_2(\infty)}(\ell_y, t) = \mathcal{V}_{y_1, y_2(\infty)}(\ell_y, t) - \mathcal{V}_{y_1, y_2(\infty)}(\ell_y, t_f), \quad (4.35)$$

where $\mathcal{V}_{y_1, y_2(\infty)}(\ell_y, t)$ and $\mathcal{V}_{y_1, y_2(\infty)}(\ell_y, t_f)$ are the pseudopotentials extracted from the action (4.32) at the current time and at the time when the black brane has already formed,

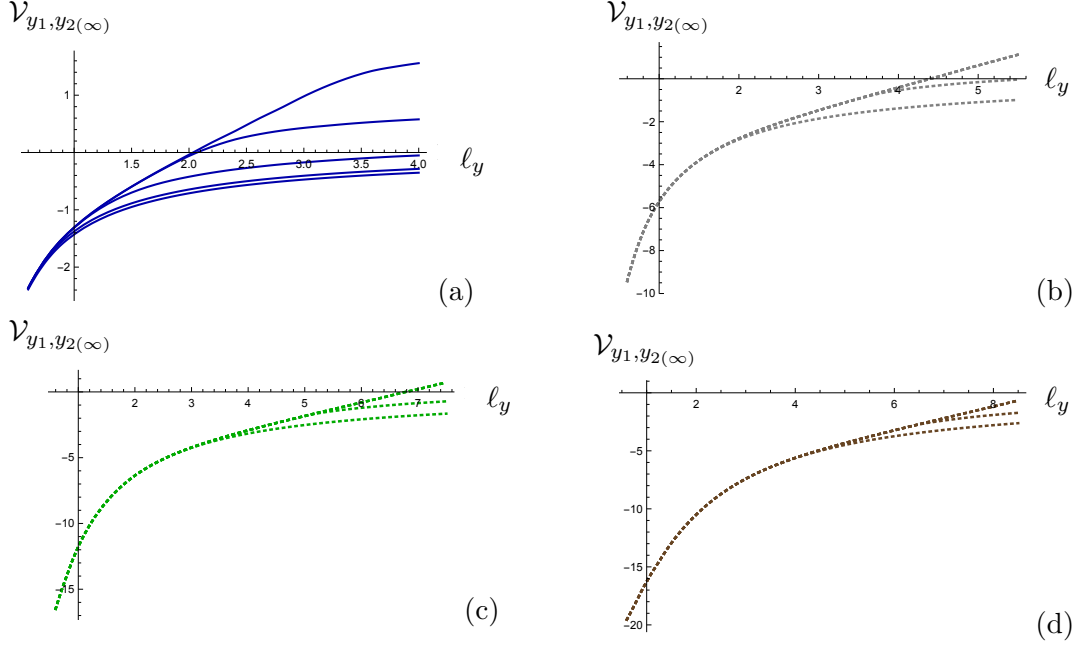


Figure 11. The pseudopotential $\mathcal{V}_{y_1, y_2(\infty)}$ as a function of the length ℓ at fixed values of t , $\nu = 1, 2, 3, 4$ ((a),(b),(c),(d), respectively). (a): we take $t = 0.1, 0.5, 0.9, 1.4, 2$ from down to top, respectively; for plots (b),(c),(d): $t = 0.4, 1.5, 2.5, 3.34, 4$ from down to top, respectively. In (2.21) we take $M = 1$.

respectively. The time dependence of $-\delta\mathcal{V}_{y_1, y_2(\infty)}(\ell_y, t)$ (taken with the negative sign) for different values of the length ℓ and ν is shown in Fig.12. One can see that the behavior of $-\delta\mathcal{V}_{y_1, y_2(\infty)}(\ell_y, t)$ is not so sharp as for $-\delta\mathcal{V}_{x, y_1(\infty)}(\ell_x, t)$ and $-\delta\mathcal{V}_{y_1, x(\infty)}(\ell_y, t)$. We note that the influence of the critical exponent on the rate of the thermalization process for $\delta\mathcal{V}_{y_1, y_2(\infty)}(\ell_y, t)$ is even higher than for $-\delta\mathcal{V}_{x, y_1(\infty)}(\ell_x, t)$ and $-\delta\mathcal{V}_{y_1, x(\infty)}(\ell_y, t)$. In all these cases the saturation time increases with ℓ and ν .

5 Thermalization times

5.1 Thermalization times of spacial Wilson loops

In this section, we compare the thermalization time for spatial Wilson loops with different orientations and its dependence on the value of the dynamical exponent ν . To simplify these estimations we consider the thin shell limit. We are interested in the value of the boundary time t_{therm} when the string profile is totally covered by the thin shell, i.e.:

$$t_{therm}(\ell) = \int_0^{z_*(\ell)} \frac{dz}{f(z)}, \quad (5.1)$$

where ℓ is the length between the string endpoints on the boundary.

In Fig.13 we plot the dependence on ℓ of the thermalization time for two configurations in the xy_1 -plane. In Fig.14(a) the behavior of the thermalization time as a function of ℓ for the configuration in the transverse y_1y_2 -plane is presented. One can see that the

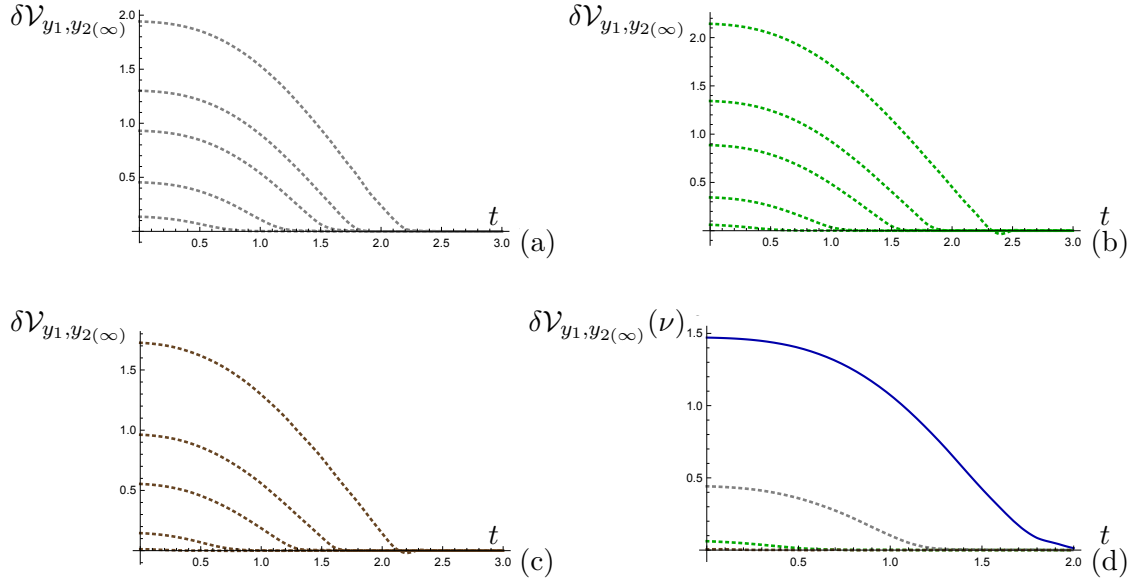


Figure 12. The time dependence of $-\delta\mathcal{V}_{y_1, y_2(\infty)}(\ell_y, t)$ on the boundary time t for different values of ℓ , $\nu = 2, 3, 4$ ((a),(b),(c), respectively). (a): $\ell = 2.2, 3, 3.85, 4.4, 5.2$ from top to down, respectively; (b): $\ell = 3, 4.1, 5.2, 6, 7.1$ from top to down, respectively; (c): $\ell = 3.4, 4.6, 5.9, 6.8, 8$ from top to down, respectively. In (d): we have shown the quantity $-\delta\mathcal{V}_{y_1, y_2(\infty)}(\ell_y, t)$ as a function of t at $\ell = 3$ for $\nu = 1, 2, 3, 4$ (from top to down, respectively). In (2.21) we take $M = 1$.

thermalization time decreases with increasing ν for all cases plotted in Fig. 13 and Fig. 14. The dependence on the length ℓ for the loop in the xy_1 -plane with the short extent in the x -direction is linear. At the same time, the dependence for the loop in the same plane, but with the short extent in the y_1 -direction, as well as for the loop in y_1y_2 -plane, is not linear for small ℓ asymptoting to the linear dependence only for large ℓ . It should be noted that the deviation from linearity strengthens with increasing ν . We also see that for the configuration in the transverse plane, the deviation of the thermalization time for the anisotropic cases from the isotropic one the thermalization time is much stronger than for the other orientations. In Fig.14(b) the comparison of thermalization times for different orientations in the case $\nu = 4$ is plotted. This plot shows that the dependence on the orientation is crucial, varying the orientation we change the order of thermalization time. This means that characteristic scale depends on the orientation. The similar behavior of the thermalization time on ℓ was observed for the thermalization time of two-point correlators in [44].

5.2 Thermalization times of different observables

It is interesting to compare the thermalization times of different observables. In our work [44] we have studied two-point correlation functions and the holographic entanglement entropy in the Lifshitz-like backgrounds. By virtue of the spatial anisotropy of the metric we had two different configurations of the correlators and entropy with respect to the

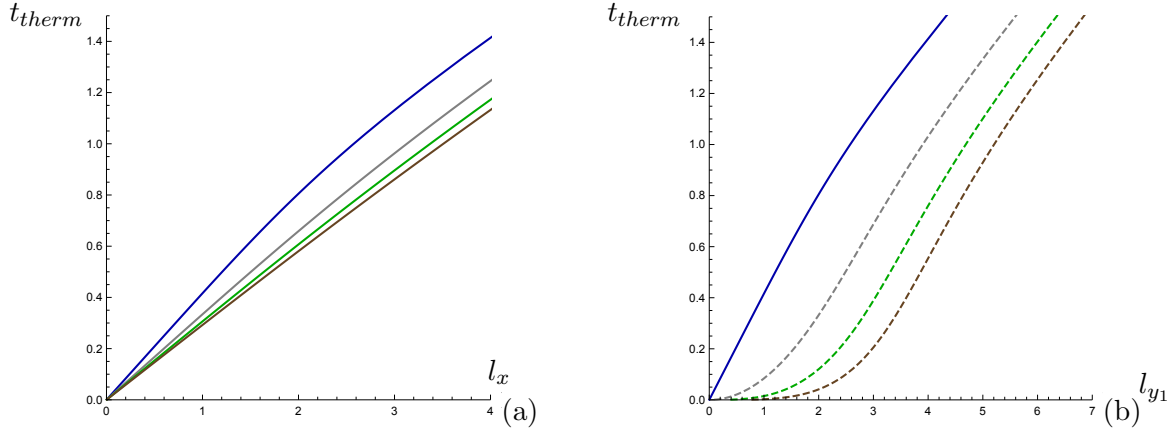


Figure 13. The thermalization time for the Wilson loop in the xy_1 -plane with a short extent in the x - and y -directions ((a) and (b), respectively). Different curves correspond to different values of $\nu = 1, 2, 3, 4$ (from top to down for each plot).

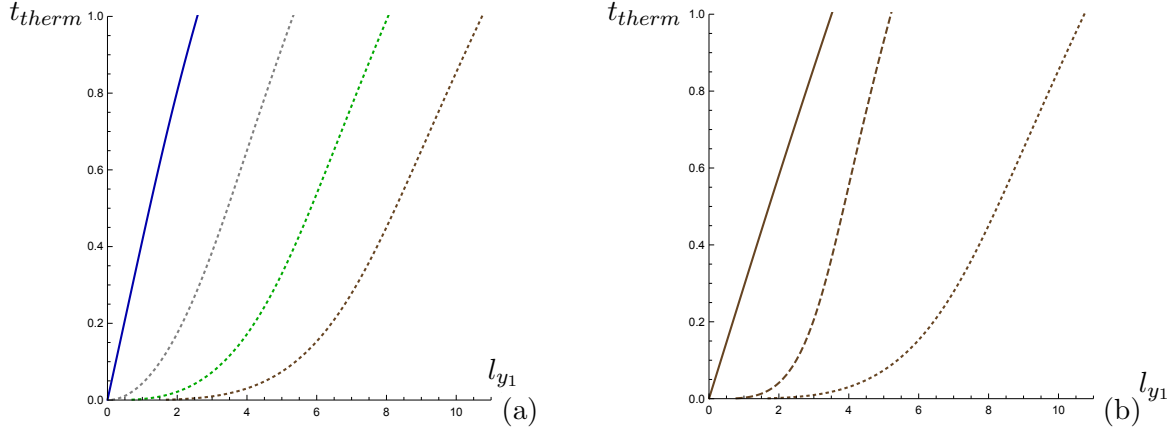


Figure 14. (a) The thermalization time as a function of ℓ for the Wilson loop in the y_1y_2 -plane, different curves correspond to different values of $\nu = 1, 2, 3, 4$ (from left to right). (b) The thermalization time as a function of ℓ for $\nu = 4$, for Wilson loops with short extents in the x - and y -directions lying in the xy_1 -plane and for the Wilson loop in the y_1y_2 -plane (from left to right).

longitudinal and transversal directions. We have observed that the entanglement entropy for a subsystem delineated in the transversal direction thermalizes faster than the two-point correlator and Wilson loop in the longitudinal one. In [44] we also have calculated thermalization times for two-point correlators. In Appendix C the additional computations for the thermalization time of the holographic entanglement entropy are given. In figure 15 we show the comparison of the thermalization times for two point correlation functions, holographic entanglement entropy and Wilson loops for different configurations.

We see that the order of the thermalization process in a certain direction is similar to

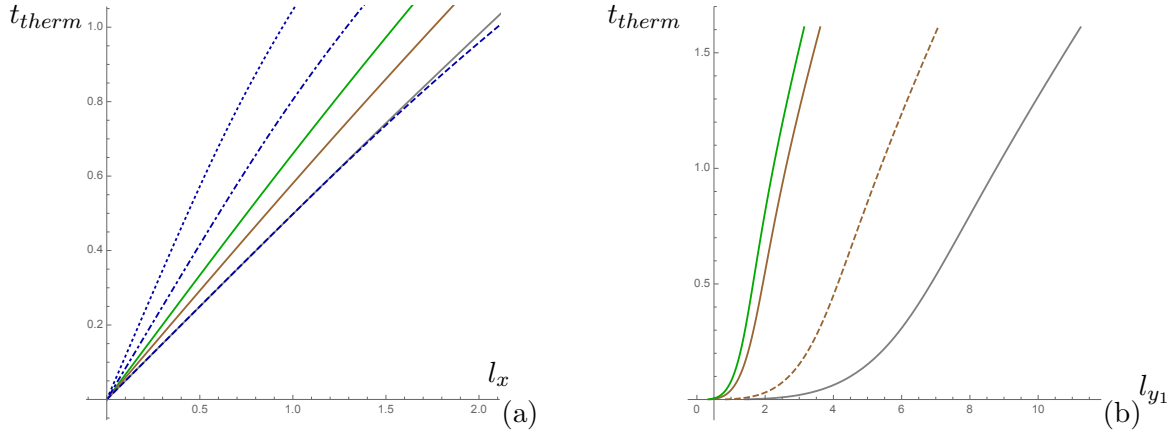


Figure 15. The thermalization times of the two-point correlators, holographic entanglement entropy and Wilson loops for different configurations. (a) The solid lines (from left to right) correspond to the entropy (green), the Wilson loop (brown) and the two-point correlator (gray) with the dependences on the longitudinal direction x in the anisotropic background with $\nu = 4$, while the dashed, dash-dotted and dotted lines represent the behaviour of the two-point correlator, Wilson loop and entropy in the isotropic spacetime, respectively. (b) The solid curves correspond to the entropy (green), the Wilson loop (brown) on the xy_1 -plane and the two-point correlator (gray) with the dependences on the transversal direction y_1 . The dashed curve corresponds to the Wilson loop on the y_1y_2 -plane. All plots in (b) are for the anisotropic background with $\nu = 4$.

the case in the isotropic and ordinary Lifshitz backgrounds [36]. The two-point correlator is the observable that thermalizes first, then we observe the thermalization of the Wilson loops, and the entanglement entropy is the observable that thermalizes last. One should be noted that the thermalization process of the Wilson loop and the entanglement entropy in the anisotropic background is faster even in the longitudinal direction than thermalization of the same observables in the isotropic case. From figure 15 (a) it is also interesting to see that the curves for the two-point correlator in the x -direction in the anisotropic background and the correlator in the isotropic spacetime match.

6 Conclusions

In this paper, we have explored the holographic scenario of the formation of the quark-gluon plasma using the Vaidya-Lifshitz bulk backgrounds, which possess spatially anisotropy. To probe the formation of the quark-gluon plasma we have used the rectangular spatial Wilson loops located on the boundary of asymptotically Lifshitz-like backgrounds. We have considered three possible configurations of Wilson loops on the boundary: the infinite rectangular strip located on the plane including one longitudinal and one transverse directions, the xy_1 -plane, with a short extent in the x - or y_1 -direction, and the infinite rectangular strip located on the transverse y_1y_2 -plane.

We have analyzed Wilson loops both for static and time-dependent cases using the static black brane and Vaidya solutions in Lifshitz-like backgrounds, respectively. The

results obtained in this paper show how the expectations of Wilson loops are modified in the presence of anisotropy in the strong coupling limit.

We have found, that at small distances, the pseudopotential derived from the Wilson loop located in the xy_1 -plane has a nontrivial dependence on the parameter ν . Namely, for $\nu > 1$ a breaking of the Coulomb phase has been observed. For Wilson loops lying in the transverse plane the Coulomb phase is unbroken, and all dependence for small ℓ is encoded in the ν dependent constant. At large ℓ all pseudopotentials are linear growing functions. Also we have found that the magnetic string tension is also affected by the anisotropic parameter ν . For the contour located on the transverse directions, the dependence of the string tension on the temperature is suppressed by anisotropy, so the magnetic string tension becomes close to a constant value. This effect is clearly seen for large ν . We have also observed interesting results for Wilson loops in the Lifshitz-Vaidya backgrounds. The effect of anisotropy parameter on the thermalization time for different orientations also has been investigated. In the $x, y_{1(\infty)}$ -case of orientation the dependence of thermalization time on scale ℓ is linearly growing function for all ν . For other orientation the dependence is not linear. In the transverse orientation this can be seen very clear. Until some critical value the dependence is slowly growing function, and after this critical value it shows the linear growth.

A common feature in the behavior of the pseudopotential is the tendency of achievement of the saturation for large values of the boundary time. The dynamical exponent also influences to the thermalization of Wilson loops, so that the value of ν increases this behavior strengthens. We have seen that the thermalization is much faster than in the AdS case. It is worth noticing that the approach to the saturation also depends on the orientation of the Wilson loop. The configuration on the transversal directions the system saturates quicker than for the contours on the xy_1 -plane.

Comparing to results for the evolution of the holographic entanglement entropy in the Lifshitz-like backgrounds in [44] we have found that the thermalization process both of the Wilson loops and the entanglement entropy is faster in the transverse direction. We have seen the similar behavior of the thermalization time as a function of ℓ for the two-point correlators in [44].

As already mentioned we have computed holographically spatial Wilson loops, pseudopotentials and spatial string tensions in the asymptotically Lifshitz-like backgrounds. A natural extension of this work is to focus on usual Wilson loops in these backgrounds and derive related expectation values, in particular, potentials of the quark interaction. Static potentials by means rectangular Wilson loops with time-like extent in static anisotropic backgrounds have been studied in [58]-[60]. Here it would be interesting to study the jet quenching described by a ratio of mean transverse momentum obtained by the parton moving through the plasma over the travelled distance. Calculations of the jet quenching parameters in anisotropic static backgrounds in the framework of the holographic duality were performed in [23],[58]-[59]. The time-like Wilson loop in the time-dependent Lifshitz-Vaidya metric are of special interest for future work⁵.

⁵One can find a consideration of time-like Wilson loops in the AdS-Vaidya background in [76].

Acknowledgments

We are grateful to Oleg Teryaev for useful discussions. A part of this work, Sect.4 and Sect.5, was done in Steklov Mathematical Institute of Russian Academy of Science by D.S. Ageev and I.Ya. Aref'eva and they are supported by the Russian Science Foundation (project 14-50-00005).

APPENDIX

A Some details on numerical solutions

Here we collect different supplementary information on numerical solutions obtained for string profiles hanging from the boundary for different orientations. In particular, we collect the string profiles behaviour for different time moments and the plots of functions $\mathfrak{b}(z)$ for each case of orientation and different ν . Function $\mathfrak{b}(z)$ is used for the renormalization of the string hanging from the boundary of the time-dependent background considered in this work.

A.1 Case 1

In Fig.16 we plot the dependence of the function \mathfrak{b} (4.12) described in Sec. 4.1.1 .

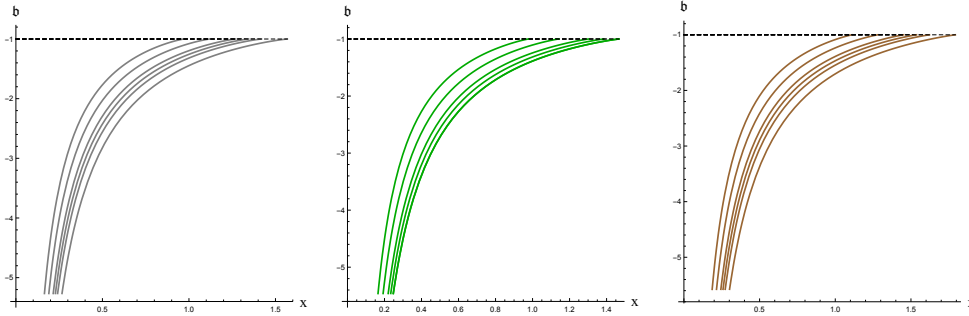


Figure 16. The dependence of the quantity $\mathfrak{b}(z)$ on the solution for $z(x)$ for $\nu = 2, 3, 4$ (from left to right). The black brane mass $M = 1$.

A.2 Case 2

In Fig.17 and 18 we plot the behaviour of string profiles for different time moments and function (4.22) respectively for orientation described in Sec. 4.1.2.

A.3 Case 3

In Fig.19 we plot string profiles for the totally transversal orientation for different values of anisotropy parameter values ν , see Sec. 4.2. We see, that the change in string profile occurs at large values of boundary time t . In Fig.20 we plot the dependence of quantity $\mathfrak{b}(z)$ defined by formula (4.33).

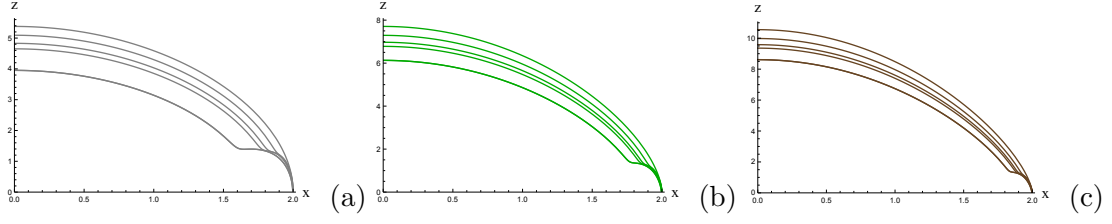


Figure 17. Profiles of the string $z(x)$, $z(1) = 0$ for different moments of the boundary time t , $\nu = 2, 3, 4$ ((a),(b),(c) respectively). The black brane mass $M = 1$.

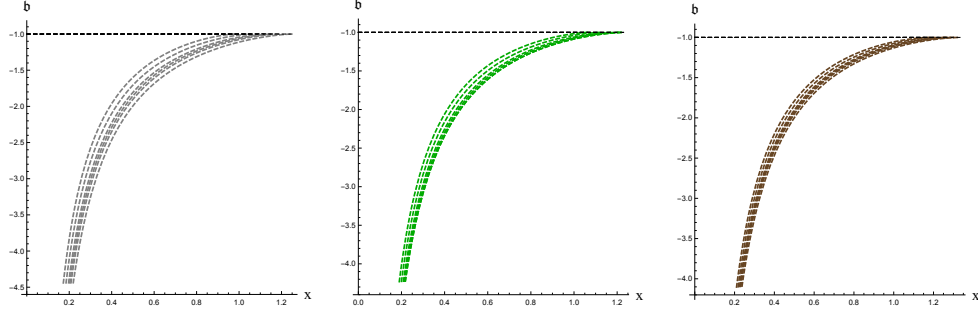


Figure 18. The dependence of the quantity $\mathbf{b}(z)$ on the solution for $z(x)$ for $\nu = 1, 2, 3$ and 4 (from left to right). The black brane mass $M = 1$.

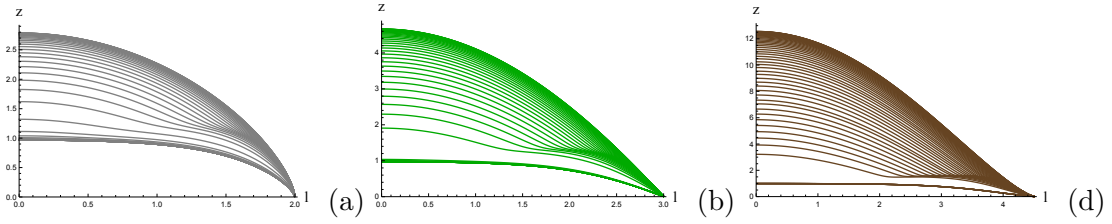


Figure 19. Profiles of the string $z(x)$, $z(2) = 0$ (blue and gray curves), $z(3) = 0$ (green curves) and $z(4.3) = 0$ (brown curves) for different moments of the boundary time, $\nu = 2, 3, 4$ ((b),(c),(d), respectively). The black brane mass $M = 1$.

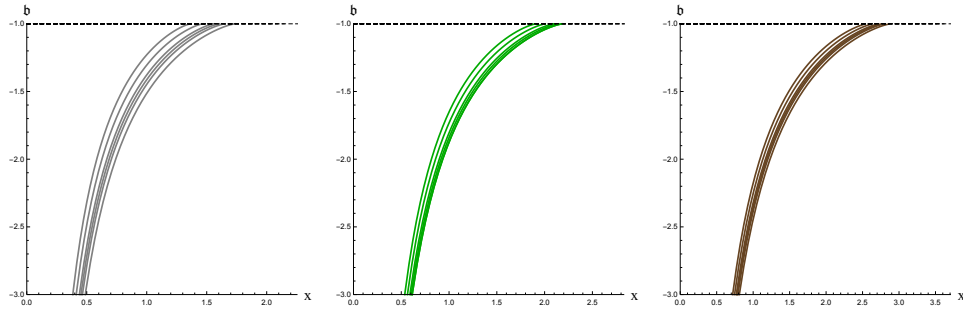


Figure 20. The dependence of the quantity $\mathbf{b}(z)$ on the solution for $z(x)$ for $\nu = 2, 3, 4$ (from left to right). The black brane mass $M = 1$.

B Asymptotics for static pseudopotentials

B.1 Rectangular strip in xy_1 -plane infinite along the y_1 -direction

The integral in (3.12) can be evaluated approximately

$$\ell_x \approx -\frac{\sqrt{\pi} z_* \Gamma\left(-\frac{1}{2\nu+2}\right)}{2(\nu+1)(3\nu+2)\Gamma\left(\frac{\nu}{2\nu+2}\right)} \left(6\nu+4+(2\nu+1)mz_*^{\frac{2}{\nu}+2}\right). \quad (\text{B.1})$$

For $\nu = 4$ we have

$$84\ell_x \approx 5.12z_* \left(28 + 9mz_*^{5/2}\right) \quad (\text{B.2})$$

and this gives

$$z_* = \ell_x \left(0.586 - 0.0495\ell_x^{5/2}m + \mathcal{O}(\ell_x^5 m^2)\right). \quad (\text{B.3})$$

Evaluating (3.14) for $\nu = 4$ we get approximately

$$\mathcal{V}_{x,y_1(\infty)} = -\frac{1}{z_*^{1/4}} \left(\frac{8\sqrt{\pi}\Gamma\left(\frac{9}{10}\right)}{\Gamma\left(\frac{2}{5}\right)} + \frac{\sqrt{\pi}\Gamma\left(\frac{9}{10}\right)}{\Gamma\left(\frac{2}{5}\right)} m z_*^{5/2} + \mathcal{O}(m^2 z_*^5) \right). \quad (\text{B.4})$$

Substituting (B.3) in (B.4) we get

$$\mathcal{V}_{x,y_1(\infty)} = -\frac{7.80}{l_x^{1/4}} \left(1 - 0.012 m l_x^{5/2} + \mathcal{O}(m^2 l_x^5)\right) \quad (\text{B.5})$$

In Figure 21 we present the comparison of the pseudopotentials given by exact formula (3.14), (3.11) and the approximated formula (B.5).

Inverting (B.1) for arbitrary ν we obtain

$$z_* = l_x \left(\frac{\Gamma\left(\frac{\nu}{2\nu+2}\right)}{2\sqrt{\pi}\Gamma\left(1 - \frac{1}{2(\nu+1)}\right)} - B_{l_x} m l_x^{\frac{2}{\nu}+2} + \mathcal{O}(\ell_x^{\frac{4}{\nu}+4} m^2) \right), \quad (\text{B.6})$$

where

$$B_{l_x} = \frac{\nu \left(\frac{\Gamma\left(\frac{\nu}{2\nu+2}\right)}{\Gamma\left(1 - \frac{1}{2(\nu+1)}\right)} \right)^{\frac{2}{\nu}+4} \Gamma\left(2 - \frac{1}{2(\nu+1)}\right)}{(\nu+1)2^{\frac{2}{\nu}+5} \pi^{\frac{1}{\nu}+\frac{3}{2}} \Gamma\left(\frac{5\nu+4}{2\nu+2}\right)}. \quad (\text{B.7})$$

The pseudopotential $\mathcal{V}_{x,y_1(\infty)}$ can be evaluated approximately

$$\mathcal{V}_{x,y_1(\infty)} = l_x^{-\frac{1}{\nu}} \left(A_{l_x} + F_{l_x} m l_x^{\frac{2}{\nu}+2} + \mathcal{O}(m^2 l_x^{\frac{4}{\nu}+4}) \right), \quad (\text{B.8})$$

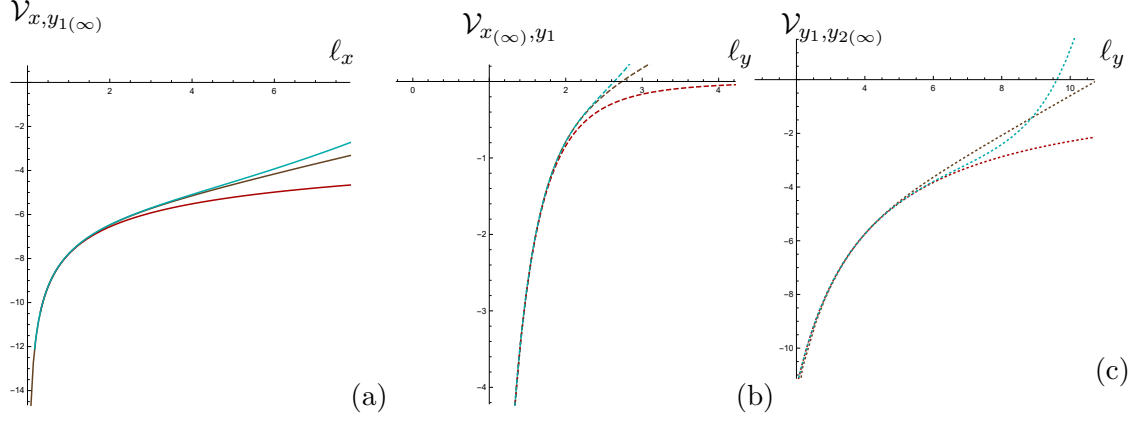


Figure 21. a) The comparison of the pseudopotentials given by exact formula (3.14) (the brown line), massless approximation (the red bottom line) and the first massive correction (the cyan top line) (B.5). b) The comparison of the pseudopotentials given by exact formula (4.25) (the brown dashed line), massless approximation (the red bottom dashed line) and the first massive correction (the cyan top dashed line) (B.15). c) The comparison of the pseudopotentials given by exact formula (3.31) (the brown dotted line), massless approximation (the red bottom dotted line) and the first massive correction (the cyan top dotted line) (B.24). For all plots $m = 0.2$.

where

$$A_{l_x} = \frac{\nu^2 \Gamma\left(-\frac{1}{2(\nu+1)}\right) \Gamma\left(1 - \frac{1}{2(\nu+1)}\right)^{\frac{1}{\nu}} \left(\Gamma\left(\frac{\nu}{2\nu+2}\right)\right)^{-1/\nu}}{2^{2-\frac{1}{\nu}} \pi^{\frac{\nu+1}{2\nu}-\frac{1}{\nu}-1} (\nu+1)^2 \Gamma\left(\frac{3\nu+2}{2\nu+2}\right)}, \quad (\text{B.9})$$

$$F_{l_x} = \frac{\csc\left(\frac{\pi}{2\nu+2}\right) \Gamma\left(-\frac{1}{2(\nu+1)}\right) \Gamma\left(1 - \frac{1}{2(\nu+1)}\right)^{-\frac{1}{\nu}-3} \left(\Gamma\left(\frac{\nu}{2\nu+2}\right)\right)^{\frac{1}{\nu}+2}}{2^{\frac{1}{\nu}+3} \pi^{\frac{\nu+1}{2\nu}-1} (\nu+2) \Gamma\left(\frac{1}{2\nu+2}\right) \Gamma\left(-\frac{\nu+2}{2\nu+2}\right)} + \frac{\Gamma\left(-\frac{1}{2(\nu+1)}\right) \Gamma\left(\frac{3\nu+2}{2\nu+2}\right) \Gamma\left(1 - \frac{1}{2(\nu+1)}\right)^{-\frac{1}{\nu}-3} \Gamma\left(2 - \frac{1}{2(\nu+1)}\right) \left(\Gamma\left(\frac{\nu}{2\nu+2}\right)\right)^{\frac{1}{\nu}+2}}{(\nu+2) 2^{\frac{1}{\nu}+3} \pi^{\frac{\nu+1}{2\nu}} \Gamma\left(-\frac{\nu+2}{2\nu+2}\right) \Gamma\left(\frac{5\nu+4}{2\nu+2}\right)}. \quad (\text{B.10})$$

For large ν one can expand the coefficients and obtain

$$\mathcal{V}_{x,y_1(\infty)} = -\frac{2\nu}{\ell_x^{1/\nu}} \left(1 - \frac{\pi^2}{24\nu^2}\right) \left(1 - \frac{1+3\nu}{3(24\nu^2 - \pi^2)} m \ell_x^{\frac{2}{\nu}+2} + \mathcal{O}(m^2 \ell_x^{\frac{4}{\nu}+4})\right). \quad (\text{B.11})$$

B.2 Rectangular strip in the xy_1 -plane infinite along the x -direction

For $\nu = 4$ the integral (3.24) can be evaluate approximately

$$\ell_y = z_*^{1/4} \left(\frac{22 \cdot 2^{4/5} \pi \Gamma\left(\frac{6}{5}\right)}{5 \Gamma\left(\frac{1}{10}\right) \Gamma\left(\frac{21}{10}\right)} + \frac{6 \cdot 2^{4/5} \pi \Gamma\left(\frac{6}{5}\right)}{5 \Gamma\left(\frac{1}{10}\right) \Gamma\left(\frac{21}{10}\right)} z_*^{5/2} + \mathcal{O}(m^2 z_*^5) \right) \quad (\text{B.12})$$

and inverting we get

$$z_* = \ell_y^4 [0.0412 - 0.0000155 m \ell_y^{10} + \mathcal{O}(m^2 \ell_y^{20})]. \quad (\text{B.13})$$

The pseudopotential for $\nu = 4$ reads

$$\mathcal{V}_{y_1, x(\infty)}(z_*) = \frac{1}{z_*} \left[-2 \frac{\sqrt{\pi} \Gamma\left(\frac{3}{5}\right)}{\Gamma\left(\frac{1}{10}\right)} + 4 \frac{\sqrt{\pi} \Gamma\left(\frac{3}{5}\right)}{\Gamma\left(\frac{1}{10}\right)} m z_*^{5/2} + \mathcal{O}(m^2 z_*^5) \right]. \quad (\text{B.14})$$

Plugging (B.13) in (B.14) we get

$$\mathcal{V}_{y_1, x(\infty)}(\ell_y) = -\frac{13.5}{\ell_y^4} (1 - 0.00031 m \ell_y^{10} + \mathcal{O}(m^2 \ell_y^{20})). \quad (\text{B.15})$$

Performing the same for arbitrary ν we have

$$z_* = l_y^\nu \left[\left(\frac{2 \pi^{1/2} \Gamma\left(\frac{1}{2\nu+2}\right)}{\nu \Gamma\left(\frac{\nu+2}{2\nu+2}\right)} \right)^\nu - \frac{\nu(\nu+2) \left(\frac{\Gamma\left(\frac{1}{2\nu+2}\right)}{\nu \Gamma\left(\frac{\nu+2}{2\nu+2}\right)} \right)^{3\nu+2}}{8^{\nu+1} \pi^{\frac{3\nu}{2}+1} (2\nu+3)} m \ell_y^{2\nu+2} + \mathcal{O}(m^2 \ell_y^{4\nu+4}) \right] \quad (\text{B.16})$$

and

$$\mathcal{V}_{y_1, x(\infty)}(\ell_y) = \frac{1}{\ell_y^\nu} (Q_{l_y} + C_{l_y} m \ell_y^{2+2\nu} + \mathcal{O}(m^2 \ell_y^{4+4\nu})), \quad (\text{B.17})$$

where

$$Q_{l_y} = \frac{2^\nu \pi^{\frac{\nu+1}{2}} \nu^{\nu+1} \Gamma\left(-\frac{\nu}{2\nu+2}\right) \Gamma\left(\frac{\nu+2}{2\nu+2}\right)^\nu}{(\nu+1) \Gamma\left(\frac{1}{2\nu+2}\right)^{\nu+1}}, \quad (\text{B.18})$$

$$C_{l_y} = -\frac{\Gamma\left(\frac{1}{2\nu+2}\right)^{\nu+1} \Gamma\left(-\frac{\nu}{2\nu+2}\right) \Gamma\left(\frac{\nu+2}{2\nu+2}\right)^{-\nu-2}}{2^{\nu+3} \nu^\nu \pi^{\frac{\nu}{2}+\frac{1}{2}} (2\nu+3)}. \quad (\text{B.19})$$

For large ν we have the expansion for (B.17)

$$\mathcal{V}_{y_1, x(\infty)}(\ell_y) = -\frac{1}{\ell_y^\nu} \left(2\pi^{1/2+\nu} - \frac{(2\nu-1)\pi^{-\nu-1} e^{\frac{24\nu-\pi^2+12}{24\nu}}}{4\nu} m \ell_y^{2+2\nu} + \mathcal{O}(m^2 \ell_y^{4+4\nu}) \right). \quad (\text{B.20})$$

B.3 Rectangular strip in $y_1 y_2$ -plane infinite along the y_2 -direction

For $\nu = 4$ the integral (3.36) can be evaluated approximately

$$\ell_y = z_*^{1/4} \left(\frac{2\sqrt{\pi}\Gamma(\frac{3}{4})}{\Gamma(\frac{5}{4})} + \frac{\sqrt{\pi}\Gamma(\frac{13}{4})}{\Gamma(\frac{15}{4})} m z_*^{5/2} + \mathcal{O}(m^2 z_*^{10}) \right) \quad (\text{B.21})$$

and this gives

$$z_* = \ell_y^4 (0.00190 - 2.52 \cdot 10^{-10} m \ell_y^{10} + \mathcal{O}(m^2 \ell_y^{20})). \quad (\text{B.22})$$

The pseudopotential for $\nu = 4$

$$\mathcal{V}_{y_1, y_2(\infty)}(z_*) = \frac{1}{z_*^{1/4}} \left(\frac{2\sqrt{\pi}\Gamma(-\frac{1}{4})}{\Gamma(\frac{1}{4})} + \frac{\sqrt{\pi}\Gamma(\frac{9}{4}) m z_*^{5/2}}{\Gamma(\frac{11}{4})} + \mathcal{O}(m^2 z_*^5) \right). \quad (\text{B.23})$$

Substituting (B.22) in (B.23) we get

$$\mathcal{V}_{y_1, y_2(\infty)} = -\frac{23.0}{\ell_y} (1 - 0.741 \cdot 10^{-9} m \ell_y^{10} + \mathcal{O}(m^2 \ell_y^{20})). \quad (\text{B.24})$$

For an arbitrary value of ν from (3.36) we have

$$z_* = \ell_y^\nu [C_1 + C_2 m \ell_y^{2\nu+2} + \mathcal{O}(m^2 \ell_y^{4+4\nu})], \quad (\text{B.25})$$

where

$$C_1 = 2^{-\nu} \nu^{-\nu} \pi^{-\nu/2} \left(\frac{\Gamma(\frac{1}{4})}{\Gamma(\frac{3}{4})} \right)^\nu \quad (\text{B.26})$$

$$C_2 = -\frac{2^{-3\nu-5} \nu^{-3\nu-1} \pi^{-\frac{3\nu}{2}-1} \Gamma(\frac{1}{4})^{3\nu+3} \Gamma(\frac{3}{4})^{-3\nu-3} \Gamma(\frac{\nu}{2} + \frac{5}{4})}{\Gamma(\frac{\nu}{2} + \frac{7}{4})}. \quad (\text{B.27})$$

The pseudopotential for general ν can be expressed as

$$\mathcal{V}_{y_1, y_2(\infty)}(z_*) = \frac{1}{4} \sqrt{\pi} \nu z_*^{-1/\nu} \left(\frac{2\Gamma(-\frac{1}{4})}{\Gamma(\frac{1}{4})} + \frac{m \Gamma(\frac{\nu}{2} + \frac{1}{4}) z_*^{\frac{\nu}{2}+2}}{\Gamma(\frac{1}{4}(2\nu+3))} + \mathcal{O}(m^2 z_*^{4+4/\nu}) \right). \quad (\text{B.28})$$

Plugging (B.25) in (B.28) we get the following formula for the pseudopotential for large ν

$$\mathcal{V}_{y_1, y_2(\infty)}(\ell_y) = -\frac{1}{\ell_y} \left(\frac{4\pi \nu^2 \Gamma(\frac{3}{4})^2}{\Gamma(\frac{1}{4})^2} - \frac{\Gamma(\frac{1}{4})^{2\nu+1} \Gamma(\frac{3}{4})^{-2\nu-1}}{2^{2\nu+\frac{5}{2}} \nu^{2\nu+\frac{3}{2}} \pi^\nu} m \ell_y^{2\nu+2} + \mathcal{O}(m^2 \ell_y^{4+4\nu}) \right). \quad (\text{B.29})$$

C Thermalization times of holographic two-point correlators and entanglement entropy

C.1 Thermalization time of two-point correlators

Under the holographic approach one can find the thermalization time t_{therm} of the two-point correlator at the scale ℓ using the Vaidya background. For this, one should consider a geodesic of a bulk particle with equal time endpoints located at the distance ℓ and find the time when the geodesic covered by the shell. In the Vaidya-Lifshitz background (2.19)-(2.20) we should study the thermalization in both longitudinal and transversal directions.

For the thermalization in the longitudinal direction we have the following relation for the length

$$\ell_x = 2z_* \int_0^1 \frac{w dw}{\sqrt{f(z_* w)(1 - w^2)}}, \quad (C.1)$$

where $w = z/z_*$ and the turning point is assumed to lie above the horizon, i.e. $z_h > z_*$.

The distance in the transversal direction is given by

$$\ell_{y_1} = 2z_*^{1/\nu} \int_0^1 \frac{w^{-1+2/\nu} dw}{\sqrt{f(wz_*)(1 - w^{2/\nu})}}. \quad (C.2)$$

The thermalization time of the two-point correlator in both directions is defined by

$$t_{therm} = z_* \int_0^1 \frac{dw}{f(z_* w)}. \quad (C.3)$$

C.2 Thermalization time of entanglement entropy

To study the thermalization of the entanglement entropy we should also consider configurations in the longitudinal and transversal directions.

The longitudinal length scale is given by

$$\ell_x = 2 \int_0^1 z_* w^{1+2/\nu} \frac{dw}{\sqrt{f(z_* w)(1 - w^{2(1+2/\nu)})}}. \quad (C.4)$$

The length for a subsystem delineated in the transversal direction is

$$\ell_{y_1} = 2z_*^{1/\nu} \int_0^1 \frac{w^{3/\nu} dw}{\sqrt{f(w, z_*)(1 - w^{2(1+2/\nu)})}}. \quad (C.5)$$

Here we are also interested in the value of the boundary time when the surface is covered by the shell, i.e. the thermalization time of the entanglement entropy has the same expression as for the two-point correlator (C.3).

References

- [1] J. Casalderrey-Solana, H. Liu, D. Mateos, K. Rajagopal, U. A. Wiedemann, Gauge/String Duality, Hot QCD and Heavy Ion Collisions, [[arXiv:1101.0618](#)].
- [2] K. G. Wilson, Confinement of Quarks, *Phys. Rev.* **D 10**, 2445 (1974).
- [3] I. Y. Arefeva, Quantum Contour Field Equations, *Phys. Lett.* **B 93**, 347 (1980).
- [4] J. M. Maldacena, Wilson loops in large N field theories, *Phys.Rev.Lett.* **80** (1998) 4859-4862; [[arXiv:hep-th/9803002](#)].
- [5] S. J. Rey, S. Theisen and J. T. Yee, Wilson-Polyakov loop at finite temperature in large N gauge theory and anti-de Sitter supergravity, *Nucl. Phys.* **B 527**, 171 (1998); [[arXiv:hep-th/9803135](#)].
- [6] A. Brandhuber, N. Itzhaki, J. Sonnenschein and S. Yankielowicz, Wilson loops in the large N limit at finite temperature, *Phys. Lett.* **B 434**, 36 (1998); [[arXiv:hep-th/9803137](#)].
- [7] J. Sonnenschein, What does the string/gauge correspondence teach us about Wilson loops?, [[arXiv:hep-th/0003032](#)].
- [8] J. Babington, J. Erdmenger, N. J. Evans, Z. Guralnik and I. Kirsch, Chiral symmetry breaking and pions in non-supersymmetric gauge/gravity duals, *Phys. Rev.* **D 69**, 066007 (2004); [[arXiv:hep-th/0306018](#)].
- [9] M. Kruczenski, D. Mateos, R. C. Myers and D. J. Winters, Towards a holographic dual of large N(c) QCD, *JHEP* **05**, 041 (2004); [[arXiv:hep-th/0311270](#)].
- [10] T. Sakai and S. Sugimoto, More on a holographic dual of QCD, *Prog.Theor.Phys.* **114**, 1083 (2006); [[arXiv:hep-th/0507073](#)].
- [11] J. Polchinski and M. J. Strassler, Deep inelastic scattering and gauge/string duality,” *JHEP* **05**, 012 (2003); [[arXiv:hep-th/0209211](#)].
- [12] A. Karch, E. Katz, D. T. Son and M. A. Stephanov, Linear confinement and AdS/QCD, *Phys. Rev.* **D 74**, 015005 (2006); [[arXiv:hep-ph/0602229](#)].
- [13] O. Andreev and V. I. Zakharov, Heavy-quark potentials and AdS/QCD, *Phys. Rev.* **D 74**, 025023 (2006); [[arXiv:hep-ph/0604204](#)].
- [14] C. D. White, The Cornell potential from general geometries in AdS / QCD, *Phys. Lett. B* **652**, 79 (2007); [[arXiv:hep-ph/0701157](#)].
- [15] U. Gursoy, E. Kiritsis, L. Mazzanti and F. Nitti, Holography and Thermodynamics of 5D Dilaton-gravity, *JHEP* **05**, 033 (2009); [[arXiv:0812.0792](#)].
- [16] B. Galow, E. Megias, J. Nian and H. J. Pirner, Phenomenology of AdS/QCD and Its Gravity Dual, *Nucl. Phys.* **B 834**, 330 (2010); [[arXiv:0911.0627](#)].
- [17] S. He, M. Huang and Q. -S. Yan, Logarithmic correction in the deformed AdS₅ model to produce the heavy quark potential and QCD beta function, *Phys. Rev.* **D 83**, 045034 (2011); [[arXiv:1004.1880](#)].
- [18] U. Gursoy, E. Kiritsis, L. Mazzanti, G. Michalogiorgakis and F. Nitti, Improved Holographic QCD, *Lect. Notes Phys.* **828**, 79 (2011); [[arXiv:1006.5461](#)].
- [19] D. S. Ageev and I. Y. Aref’eva, Holographic thermalization in a quark confining background, *J. Exp. Theor. Phys.* **120**, 3, 436 (2015); [[arXiv:1409.7558](#)].

- [20] I. Ya. Aref'eva, Holographic approach to quark-gluon plasma in heavy ion collisions, *Phys. Usp.* **57** (2014) 527.
- [21] O. DeWolfe, S. S. Gubser, C. Rosen and D. Teaney, Heavy ions and string theory, *Prog. Part. Nucl. Phys.* **75**, 86 (2014); [[arXiv:1304.7794](#)].
- [22] M. Strickland, Thermalization and isotropization in heavy-ion collisions, *Pramana* **84**, (2015) 671; [[arXiv:1312.2285](#)].
- [23] D. Giataganas, Observables in Strongly Coupled Anisotropic Theories, *PoS Corfu* **2012**, 122 (2013); [[arXiv:1306.1404](#)].
- [24] S. S. Gubser, S. S. Pufu and A. Yarom, Entropy production in collisions of gravitational shock waves and of heavy ions, *Phys. Rev. D* **78** (2008) 066014; [[arXiv:0805.1551](#)].
- [25] J. L. Albacete, Y. V. Kovchegov and A. Taliotis, Modeling heavy ion collisions in AdS/CFT, *JHEP* **07** (2008) 100; [[arXiv:0805.2927](#)].
- [26] L. Alvarez-Gaume, C. Gomez, A. Sabio Vera, A. Tavanfar and M. A. Vazquez-Mozo, Critical formation of trapped surfaces in the collision of gravitational shock waves, *JHEP* **02** (2009) 009; [[arXiv:0811.3969](#)].
- [27] P. M. Chesler and L. G. Yaffe, Horizon formation and far-from-equilibrium isotropization in supersymmetric Yang-Mills plasma, *Phys. Rev. Lett.* **102** (2009) 211601; [[arXiv:0812.2053](#)].
- [28] S. Lin and E. Shuryak, Grazing collisions of gravitational shock waves and entropy production in heavy ion collision, *Phys. Rev. D* **79** (2009) 124015; [[arXiv:0902.1508](#)].
- [29] I. Ya. Aref'eva, A. A. Bagrov and E. A. Guseva, Critical formation of trapped surfaces in the collision of non-expanding gravitational shock waves in de Sitter space-time, *JHEP* **12** (2009) 009; [[arXiv:0905.1087](#)].
- [30] P. M. Chesler and L. G. Yaffe, Holography and colliding gravitational shock waves in asymptotically AdS5 spacetime, *Phys. Rev. Lett.* **106** (2011) 021601; [[arXiv:1011.3562](#)].
- [31] I. Ya. Aref'eva, A. A. Bagrov and E. O. Pozdeeva, Holographic phase diagram of quark-gluon plasma formed in heavy-ions collisions, *JHEP* **05** (2012) 117; [[arXiv:1201.6542](#)].
- [32] E. Kiritsis and A. Taliotis, Multiplicities from black-hole formation in heavy-ion collisions, *JHEP* **04** (2012) 065; [[arXiv:1111.1931](#)].
- [33] I. Ya. Aref'eva, E. O. Pozdeeva and T.O. Pozdeeva, Holographic estimation of multiplicity and membranes collision in modified spaces AdS_5 , *Theor. Math.Phys.* (2013) 176, 861; [[arXiv:1401.1180v1](#)].
- [34] P. Vaidya, The External Field of a Radiating Star in General Relativity, *Curr. Sci.* **12** (1943) 183.
- [35] V. Balasubramanian, A. Bernamonti, J. de Boer, N. Copland, B. Craps, E. Keski-Vakkuri, B. Muller and A. Schafer et al., Holographic thermalization, *Phys. Rev. D* **84** (2011) 026010; [[arXiv:1103.2683](#)].
- [36] V. Keranen, E. Keski-Vakkuri and L. Thorlacius, Thermalization and entanglement following a non-relativistic holographic quench, *Phys. Rev. D* **85**, 026005 (2012); [[arXiv:1110.5035](#)].
- [37] I. Ya. Aref'eva and I. V. Volovich, On holographic thermalization and dethermalization of quark-gluon plasma; [[arXiv:1211.6041](#)].
- [38] I. Ya. Aref'eva and A. A. Golubtsova, Shock waves in Lifshitz-like spacetimes, *JHEP* **1504** (2015) (011); [[arXiv:1410.4595](#)].

- [39] M. Taylor, Non-relativistic holography; [[arXiv:0812.0530](#)].
- [40] T. Azeyanagi, W. Li and T. Takayanagi, On string theory duals of Lifshitz-like fixed points, *JHEP* **06** (2009) 084; [[arXiv:0905.0688](#)].
- [41] D. Mateos, D. Trancanelli, Thermodynamics and instabilities of a strongly coupled anisotropic plasma, *JHEP* **07** (2011) 054; [[arXiv:1106.1637](#)].
- [42] S. Kachru, X. Liu and M. Mulligan, Gravity duals of Lifshitz-like fixed points, *Phys. Rev. D* **78** (2008) 106005; [[arXiv:0808.1725](#)].
- [43] I. Ya. Aref'eva, Formation time of quark-gluon plasma in heavy-ion collisions in the holographic shock wave model, *Theor. Math. Phys.*, 184:3 (2015), 1239-1255; [[arXiv:1503.02185](#)].
- [44] I. Y. Aref'eva, A. A. Golubtsova and E. Gourgoulhon, Analytic black branes in Lifshitz-like backgrounds and thermalization, *JHEP* **09** (2016) 142; [[arXiv:1601.06046](#)].
- [45] <http://sagemanifolds.obspm.fr/>
- [46] <http://www.sagemath.org/>
- [47] U. H. Danielsson and L. Thorlacius, Black holes in asymptotically Lifshitz spacetime, *JHEP* **03**, (2009) 070; [[arXiv:0812.5088](#)].
- [48] R. B. Mann, Lifshitz Topological Black Holes, *JHEP* **06**, 075 (2009); [[arXiv:0905.1136](#)].
- [49] D. W. Pang, A Note on Black Holes in Asymptotically Lifshitz Spacetime, *Commun.Theor.Phys.* **62**, 265 (2014); [[arXiv:0905.2678](#)].
- [50] P. Koroteev and A. V. Zayakin, Wilson Loops in Gravity Duals of Lifshitz-like Theories, [[arXiv:0909.2551](#)].
- [51] W. Fischler and S. Kundu, Strongly Coupled Gauge Theories: High and Low Temperature Behavior of Non-local Observables, *JHEP* **05** (2013) 098; [[arXiv:1212.2643](#)].
- [52] T. Andrade, Y. Lei and S. F. Ross, Scattering amplitudes in Lifshitz spacetime, *Class.Quant.Grav.*, 31 (2014) 21, 215002; [[arXiv:1406.6389](#)].
- [53] K. B. Fadafan, Drag force in asymptotically Lifshitz spacetimes, [[arXiv:0912.4873](#)].
- [54] K. Bitaghsir Fadafan and F. Saiedi, Holographic Schwinger effect in non-relativistic backgrounds, *Eur. Phys. J. C* **75**, 12, 612 (2015); [[arXiv:1504.02432](#)].
- [55] T. R. Araujo and H. Nastase, Non-Abelian T-duality for nonrelativistic holographic duals, *JHEP* **11**, (2015) 203; [[arXiv:1508.06568](#)].
- [56] K.B. Fadafan and H. Soltanpanahi, Energy loss in a strongly coupled anisotropic plasma, *JHEP* **10** (2012) 085; [[arXiv:1206.2271](#)].
- [57] M. Chernoiff, D. Fernandez, D. Mateos and D. Trancanelli, Drag force in a strongly coupled anisotropic plasma, *JHEP* **08** (2012) 100; [[arXiv:1202.3696](#)].
- [58] D. Giataganas, Probing strongly coupled anisotropic plasma, *JHEP* **07** (2012) 031; [[arXiv:1202.4436](#)].
- [59] M. Chernoiff, D. Fernandez, D. Mateos and D. Trancanelli, Jet quenching in a strongly coupled anisotropic plasma, *JHEP* **08** (2012) 041; [[arXiv:1203.0561](#)].
- [60] A. Rebhan and D. Steineder, Probing Two Holographic Models of Strongly Coupled Anisotropic Plasma, *JHEP* **08**, (2012) 020; [[arXiv:1205.4684](#)].

- [61] K. B. Fadafan, D. Giataganas and H. Soltanpanahi, The imaginary part of the static potential in strongly coupled anisotropic plasma, *JHEP* **11** (2013) 107; [[arXiv:1306.2929](#)].
- [62] S. Chakraborty, S. Chakraborty and N. Haque, Brownian motion in strongly coupled, anisotropic Yang-Mills plasma: a holographic approach, *Phys. Rev. D* **89** (2014) 066013; [[arXiv:1311.5023](#)].
- [63] D. Giataganas and H. Soltanpanahi, Heavy quark diffusion in strongly coupled anisotropic plasmas, *JHEP* **06** (2014) 047; [[arXiv:1312.7474](#)].
- [64] L. Cheng, X.-H. Ge and S.-J. Sin, Anisotropic plasma with a chemical potential and scheme-independent instabilities, *Phys. Lett. B* **734** (2014) 116; [[arXiv:1404.1994](#)].
- [65] T. R. Araujo, “Revisiting Wilson loops for nonrelativistic backgrounds,” *Phys. Rev. D* **92**, no. 12, 126007 (2015) doi:10.1103/PhysRevD.92.126007 [[arXiv:1509.02011 \[hep-th\]](#)].
- [66] I. Arefeva, NonAbelian Stokes formula, *Theor. Math. Phys.* **43**, 353 (1980).
- [67] G. S. Bali, J. Fingberg, U. M. Heller, F. Karsch and K. Schilling, The Spatial string tension in the deconfined phase of the (3+1)-dimensional SU(2) gauge theory, *Phys. Rev. Lett.* **71**, 3059 (1993); [[arXiv:hep-lat/9306024](#)].
- [68] P. Petreczky, Lattice QCD at non-zero temperature, *J. Phys. G* **39**, 093002 (2012); [[arXiv:1203.5320](#)].
- [69] A. Simonov, [http : //195.178.214.34/ps/1248/article_18874.pdf](http://195.178.214.34/ps/1248/article_18874.pdf)
- [70] J. Alanen, K. Kajantie and V. Suur-Uski, Spatial string tension of finite temperature QCD matter in gauge/gravity duality, *Phys. Rev. D* **80**, 075017 (2009); [[arXiv:0905.2032](#)].
- [71] O. Andreev and V. I. Zakharov, The Spatial String Tension, Thermal Phase Transition, and AdS/QCD, *Phys. Lett. B* **645**, 437 (2007); [[arXiv:hep-ph/0607026](#)].
- [72] O. Andreev, The Spatial String Tension in the Deconfined Phase of SU(N) Gauge Theory and Gauge/String Duality, *Phys. Lett. B* **659**, 416 (2008); [[arXiv:0709.4395](#)].
- [73] O. Andreev, Some Multi-Quark Potentials, Pseudo-Potentials and AdS/QCD, *Phys. Rev. D* **78**, 065007 (2008); [[arXiv:0804.4756](#)].
- [74] A. Dumitru, Y. Nara and E. Petreska, Magnetic flux loop in high-energy heavy-ion collisions, *Phys. Rev. D* **88**, 5, 054016 (2013); [[arXiv:1302.2064](#)].
- [75] A. Dumitru, T. Lappi and Y. Nara, Structure of longitudinal chromomagnetic fields in high energy collisions, *Phys. Lett. B* **734**, 7 (2014); [[arXiv:1401.4124](#)].
- [76] M. Ali-Akbari, F. Charmchi, A. Davody, H. Ebrahim and L. Shahkarami, Evolution of Wilson loop in time-dependent N=4 super Yang-Mills plasma, *Phys. Rev. D* **93**, 8, 086005 (2016); [[arXiv:1510.00212](#)].